

AUTOMATIC AND SIMULTANEOUS
CORRELATION OF MULTIPLE
WELL LOGS

by
Loralee F. Wheeler

© Copyright by Lorelee F. Wheeler, 2015

All Rights Reserved

A thesis submitted to the Faculty and the Board of Trustees of the Colorado School of Mines in partial fulfillment of the requirements for the degree of Master of Science (Geophysics).

Golden, Colorado

Date _____

Signed: _____

Loralee F. Wheeler

Signed: _____

Dr. Dave Hale
Thesis Advisor

Golden, Colorado

Date _____

Signed: _____

Dr. Terence K. Young
Professor and Head
Department of Geophysics

ABSTRACT

Well log correlation is an important step in geophysical interpretation, but as the number of wells increases, so does the complexity of the correlation process. I propose a new method for automatic and simultaneous well log correlation that provides an optimal alignment of all logs, and in addition, is relatively insensitive to large measurement errors common in well logs. First, for any number of well logs, we use a new variant of the dynamic warping method, requiring no prior geologic information, to find for each pair of logs a set of corresponding depths. Depths in one log may have one or more corresponding depths in another log, and many such pairs of corresponding depths can be found for any pair of well logs. Requiring consistency among all such pairwise correlations gives rise to an overdetermined system of equations, with unknown relative geologic time (RGT) shifts to be computed for each log sample. A least-squares solution of these equations, found using the conjugate gradient method, yields for every well log a sequence of RGT shifts that optimally align all well logs. This solution is not unique because aligned logs remain aligned if they are shifted, stretched, or squeezed vertically. Therefore, we constrain these shifts, for each RGT, to have zero mean over all logs.

TABLE OF CONTENTS

ABSTRACT	iii
LIST OF FIGURES AND TABLES	v
ACKNOWLEDGMENTS	vii
CHAPTER 1 INTRODUCTION	1
CHAPTER 2 PAIRWISE WELL LOG CORRELATION	5
2.1 Alignment errors	5
2.2 Replacing missing data	10
2.3 Accumulation and backtracking	11
CHAPTER 3 SIMULTANEOUS MULTI-WELL LOG CORRELATION	13
3.1 Computing shifts	14
3.2 Removing unnecessary stretching and squeezing	18
3.3 Updating relative geologic time	22
3.4 Reparameterization of shifts	23
3.5 Missing data	26
3.6 Analyzing log correlations	27
3.7 Multiple log types	30
CHAPTER 4 CONCLUSIONS	37
4.1 Future work	38
REFERENCES CITED	39

LIST OF FIGURES AND TABLES

Figure 1.1	13 Teapot Dome density logs before (a) and after (b) automatic simultaneous correlation.	2
Figure 1.2	Locations of 13 Teapot Dome density logs overlain on a constant-time slice (at one second) of a corresponding 3D seismic image (a). Line segments denote pairs of logs to be correlated (b).	3
Figure 2.1	(a) Alignment errors computed from subsets of logs $I = 1$ and $J = 2$ with the optimal sequence of (i, j) pairs overlain in (b). The blue line denotes sample $j = 1237$ and the yellow line denotes sample $i = 1239$. The pair $(i, j) = (1239, 1237)$ is not on the optimal path.	6
Figure 2.2	Two possible warping paths a and b in the original ij -coordinate system (a) and in the new kl -coordinate system (b).	7
Figure 2.3	Normalized alignment errors for logs $I = 1$ and $J = 2$, computed on the kl -coordinate system (a), where the blue line denotes sample $j = 1237$ and the yellow line denotes sample $i = 1239$. Alignment errors were computed for $p = \frac{1}{8}$ (b), $p = \frac{1}{2}$ (c), and $p = 2$ (d), and their respective optimal paths overlain in white. As p increases, large errors dominate and result in erroneous warping paths.	9
Figure 2.4	New computational stencil on a close up view of alignment errors computed for density logs $I = 1$ and $J = 2$. Alignment errors $e_{IJ}[k, l]$ are computed only where $k + l$ is even.	11
Figure 2.5	Three density log pairs before (a, b, c) and after (d, e, f) warping. Log indices (I, J) are denoted in black and red, corresponding to the colors of the logs.	12
Figure 3.1	Each depth z_i in log I has one or more corresponding depths z_j in log J . For such pairs of depths, log values $f(z_i, I)$ and $f(z_j, J)$ should be similar.	15
Figure 3.2	Aligned logs (a) remain aligned after being squeezed and shifted (b). . . .	19

Figure 3.3	A close-up of 13 depth functions $z(\tau, l) = \tau - r(\tau, l)$ (a). Rapid changes in depth for consecutive relative geologic times (red arrow) imply vertical squeezing of the logs and rapid changes in relative geologic time for consecutive depths (blue arrow) imply vertical stretching of the logs. After constraining the average RGT shift over the logs to be zero, each $z(\tau, l)$ is nearly diagonal (b).	22
Figure 3.4	13 Teapot Dome density logs (a) aligned using only static shifts (b). . . .	25
Figure 3.5	13 Teapot Dome density logs before (a) and after (b) automatic simultaneous correlation. A close-up of aligned density layers between RGT $\tau = 0.78 - 1.2$ (c) shows that thin density layers are aligned consistently among the logs.	28
Figure 3.6	For each RGT, absolute deviation (c) is computed by subtracting the median density (b) from the aligned logs (a). High absolute deviations may indicate areas of less reliable correlations.	29
Figure 3.7	13 density (a), 11 porosity (b), and 5 velocity (c) logs after simultaneous correlation of all three log types.	33
Figure 3.8	Median density (a), porosity (b), and velocity (c) as functions of RGT. . . .	33
Figure 3.9	Absolute deviation of density (a), porosity (b), and velocity (c).	34
Figure 3.10	Median absolute deviation of density (a), porosity (b), and velocity (c) as functions of RGT.	34
Figure 3.11	Cross section (a) of six Teapot Dome density logs with interpretation of three sets of corresponding depths, found during simultaneous correlation of density, porosity, and velocity logs. Location of the cross section is denoted by line segments (b) overlain on a constant-time slice (at one second) of a corresponding 3D seismic image. The cross section runs from A to A', passing through the apex of the anticline.	35
Figure 3.12	Stratigraphic column for Teapot Dome field provided by Rocky Mountain Oilfield Test Center. Green lithologies represent shale, blue represent limestone, yellow represent sandstone-dominated intervals, and pink represent basement rock.	36
Table 3.1	Median absolute deviation (MAD) for different alignments of the 13 density logs in Figure 3.5a, computed using various L_p -norms in alignment error equation 2.4.	30

ACKNOWLEDGMENTS

I would first like to thank my husband Kyle for his patience and support throughout my studies as well as my family for their endless support. I would also like to thank my advisor Dr. Dave Hale for his continued guidance and support. His insights have been invaluable to my research and his enthusiasm has made this an enjoyable experience. I have greatly enjoyed my time at the Center for Wave Phenomena and would like to thank the faculty and staff of CWP. I would especially like to thank Pam Kraus for handling any administrative issues, but more so for being a wonderful friend who is always willing to lend an ear. Thanks also to the Rocky Mountain Oilfield Test Center, a facility of the U.S. Department of Energy, for providing the 3D seismic image and well logs used in this study.

CHAPTER 1

INTRODUCTION

Well logs have been used for decades as a means to record various rock properties within the subsurface. Examples of such measurements include gamma ray intensity, electrical resistivity, and sonic velocity. Rock property measurements at each depth in a well log contain information about sediment type at that depth. Analyzing multiple log types simultaneously helps one to better interpret lithology within a well. These interpretations, however, are localized to their respective well locations because geologic structure varies spatially.

To estimate geologic structure between well locations, one uses well log correlation, which is the process of determining corresponding depths among multiple well logs. A single set of such corresponding depths often represents a single geologic time in which sediments with similar properties were deposited over large areas. We can therefore view well log correlation as the task of mapping each well log from depth to geologic time. An example of this mapping is illustrated in Figure 1.1, where we use the phrase “relative geologic time” (RGT) to indicate that the geologic time scale used here is arbitrary. We know only that sediments with greater relative geologic time were deposited before those with lesser RGT. For each RGT in Figure 1.1, we have a set of 13 corresponding depths, one for each well log.

Historically, well log correlation was a manual task in which a geologist would line up print-outs of several well logs and draw lines that denote corresponding geologic intervals across logs. Manual log correlations depend on the individual correlating the logs. This is because the geologic intervals we see are dependent upon the extent of our prior geologic knowledge, which implies that manual well log correlation is vastly subjective. This is one reason why automatic log correlation methods began to surface in the mid 1960s. The development of such methods can also be attributed to the rapidly increasing number of well logs being recorded.

Although a small number of well logs can be manually correlated by interpreters in a matter of minutes, this task becomes factorially more difficult as the number of logs increases. For example, for any 13 well logs, such as those shown in Figure 1.1a, $78 = \frac{13 \times (13-1)}{2}$ pairwise correlations can be made, as indicated by the 78 edges (line segments) in the graph shown in Figure 1.2b. However, in this same graph there exist over five billion cycles (distinct walks along three or more edges, beginning and ending at the same vertex, without repetition). The number of cycles N_c among L well logs is

$$N_c = \left(\prod_{l=3}^L l \right) \left(\sum_{l=3}^L \frac{1}{l} \right). \quad (1.1)$$

To see why this large number of cycles poses a problem in well log correlation, suppose that in pairwise correlations of logs we find that a depth z_i in log I corresponds to another depth z_j in log J , which in turn corresponds to a third depth z_k in log K . Then, in the

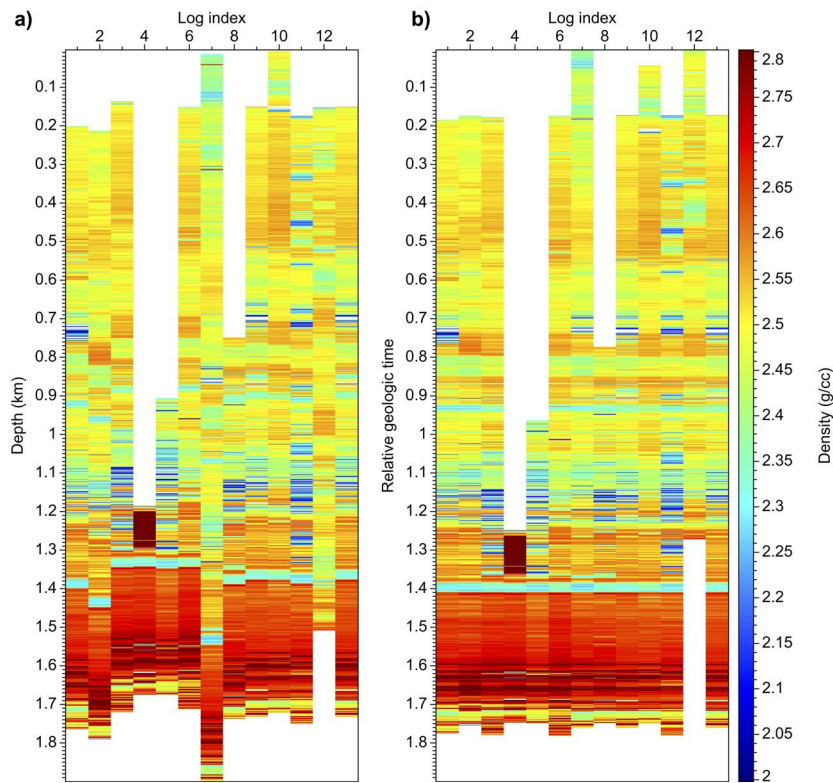


Figure 1.1: 13 Teapot Dome density logs before (a) and after (b) automatic simultaneous correlation.

pairwise correlation of logs I and K , we should find that depth z_i corresponds to depth z_k . Imposing this sort of constraint for all five billion cycles is an impossible task for human interpreters to perform in pairwise correlation of 13 logs. Moreover, because the number of cycles (constraints) grows factorially with the number of logs, this task is usually infeasible even for computers.

To reduce subjectivity and computation time, several methods for automatic correlation have been developed. These methods attempt to solve two main problems: correlation of a single pair of well logs and correlation of many well logs. For a single pair of well logs, crosscorrelation methods, such as that described by Rudman & Lankston (1973), compute correlation values over a sliding window using a crosscorrelation function. The correlation lag with the maximum value is taken to be optimal. Such crosscorrelation algorithms require modifications in cases where bed thicknesses vary between the logs and fall short when logs contain gaps in geologic time due to faults or erosion.

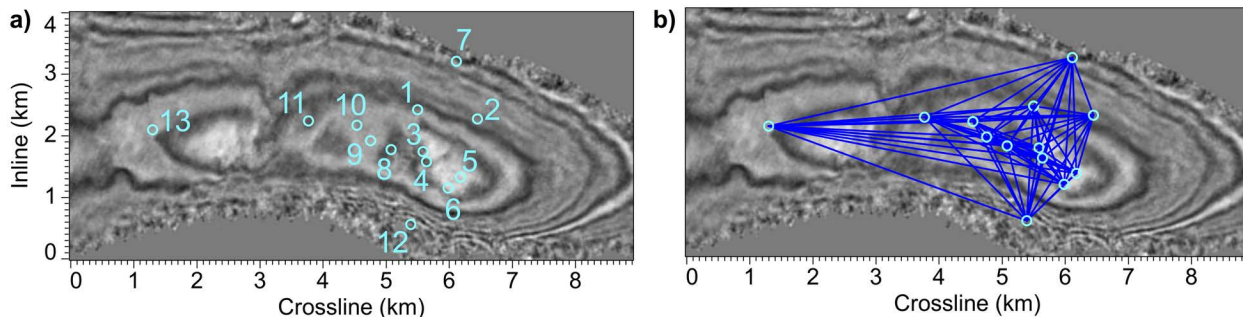


Figure 1.2: Locations of 13 Teapot Dome density logs overlain on a constant-time slice (at one second) of a corresponding 3D seismic image (a). Line segments denote pairs of logs to be correlated (b).

With these shortcomings in mind, Smith & Waterman (1980) developed a dynamic waveform matching approach, inspired by Waterman’s work in genetic sequence evolution, that finds an optimal alignment between any two well logs, including those with gaps in geologic sequences. Dynamic warping has since been a key aspect of many well log correlation methods. One such method, developed by Wu & Nyland (1987), performs pairwise well

log correlation in two main steps: contact recognition and interval identification. Contact recognition uses a statistical approach to partition a log into distinct segments that highlight contacts between beds. Interval identification uses dynamic warping to align corresponding segments among two well logs. Any of the aforementioned methods could be used to correlate any of the 78 log pairs represented by line segments in Figure 1.2b.

For correlating more than two well logs, many different approaches exist. The method developed by Le Nir *et al.* (1998) uses the most geologically complete well as a key well to which all other well logs are aligned via dynamic warping. The authors also provide a method that correlates logs sequentially along some correlation path, updating the key well after each correlation. Alternatively, Fang & Chen (1992) and Kovalevskiy *et al.* (2007) propose divide-and-conquer methods for correlating multiple well logs. In these methods, correlations are first performed for the three pairs that can be formed from any three logs. After an acceptable alignment is found, a larger number of logs are correlated using the alignment of the previous well logs as constraints for the new correlations. This process of increasing the number of logs in the correlation is continued until all logs have been aligned. Due to the propagation of error in such methods, the final correlation of all logs depends on the order in which they are correlated.

In this thesis I propose a method for automatically and simultaneously correlating any number of well logs. This method is relatively insensitive to large measurement errors that are common in well logs and provides a globally optimal (least-squares best) alignment of all logs. Using a subset of 13 density logs from Teapot Dome as an example, Chapter 2 explains our modifications to the dynamic warping algorithm and shows how it can be used to find corresponding depths for any pair of logs. Chapter 3 develops a method for using these corresponding depths to find shifts, for every depth in every log, that optimally align all logs. In the last section of Chapter 3, we extend our correlation method to include simultaneous log correlation for multiple log types.

CHAPTER 2

PAIRWISE WELL LOG CORRELATION

In general, the range of depths sampled within a set of well logs varies. Therefore, before log correlation, we resample all logs such that each log has $N_z = (z_{\max} - z_{\min})/\Delta z + 1$ samples, where z_{\min} and z_{\max} denote the minimum and maximum depths sampled in all logs and Δz is a specified sampling interval. In practice, data are commonly missing in well logs due to gaps in acquisition, and null values serve as placeholders for any missing data in a log. For the Teapot Dome example shown in Figure 1.1, we chose a depth sampling interval $\Delta z = 1$ m.

In this chapter, I describe how our modified dynamic warping algorithm can be used to find corresponding depths in any log pair. I first describe how to compute alignment errors between two well logs so that no manual interpretation is required. I then describe how to handle the special case of computing alignment errors where one of the two logs has missing data. Finally, I describe how to find a sequence of corresponding depths that optimally aligns the two logs.

2.1 Alignment errors

In automatic well log correlation, dynamic warping is commonly used to compute a sequence of pairs of depth indices (i, j) , called a path, that optimally aligns a pair of well logs (Le Nir *et al.*, 1998; Lineman *et al.*, 1987; Smith & Waterman, 1980). The first step in finding this optimal path is to compute alignment errors for each sample $f[i, I]$ of log I and each sample $f[j, J]$ of log J as follows:

$$e_{IJ}[i, j] \equiv |f[i, I] - f[j, J]|^p, \quad (2.1)$$

for $i = 0, 1, \dots, N_z - 1$ and $j = 0, 1, \dots, N_z - 1$,

where I and J are indices of two logs, i and j are indices of depths sampled in these two

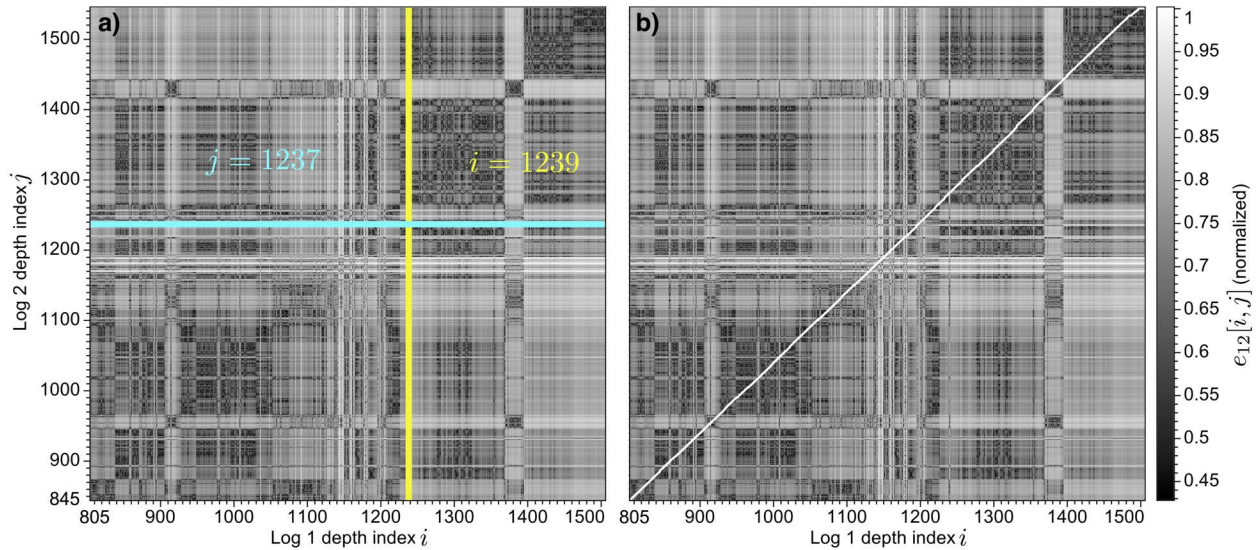


Figure 2.1: (a) Alignment errors computed from subsets of logs $I = 1$ and $J = 2$ with the optimal sequence of (i, j) pairs overlain in (b). The blue line denotes sample $j = 1237$ and the yellow line denotes sample $i = 1239$. The pair $(i, j) = (1239, 1237)$ is not on the optimal path.

logs, and p is any positive value. Alignment errors computed for density logs 1 and 2 from Teapot Dome are shown in Figure 2.1. The horizontal white lines of large alignment errors near index $j = 1190$ are due to large measurement errors in log $J = 2$ near 1.19 km depth.

Beginning at $(i = 0, j = 0)$, alignment errors are accumulated along all possible paths from the lower-left to the upper-right of the ij -grid to find accumulated alignment errors at the end of each path. The accumulated alignment error at the end of the minimal-error path is defined as

$$D_{IJ} = \min_{path} \sum_{(i,j) \in path} e_{IJ}[i, j]. \quad (2.2)$$

The solid white curve in Figure 2.1b represents the optimal sequence of (i, j) pairs (the optimal path) for density logs $I = 1$ and $J = 2$. Each point on this path represents a pair (i, j) of corresponding depths in logs $I = 1$ and $J = 2$.

Although there are many possible warping paths, Figure 2.2a shows just two possible paths a and b for logs I and J on the ij -coordinate system. A path along the diagonal of the

ij -grid, from $(0, 0)$ to $(N_z - 1, N_z - 1)$, implies that log values for indices $i = 0, 1, 2, \dots, N_z - 1$ in log I are already aligned with those for indices $j = 0, 1, 2, \dots, N_z - 1$ in log J , respectively. Path b lies relatively close to the diagonal of the ij -grid, which implies that the pairs of log values in path b are reasonably well-aligned without warping. However, for path b , depths in log I are mostly greater than corresponding depths in log J because this path lies mostly below the diagonal. The opposite is true for path a ; depths in log I are shallower than corresponding depths in log J . The optimal path for logs $I = 1$ and $J = 2$ in Figure 2.1b is similar to path a in that it too lies above the diagonal.

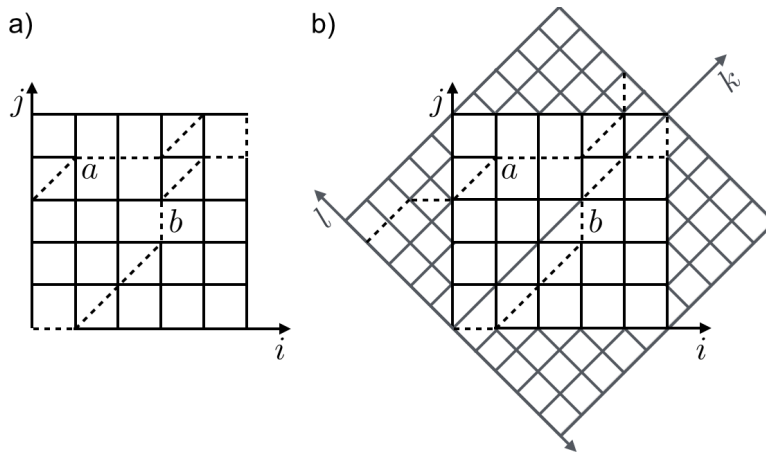


Figure 2.2: Two possible warping paths a and b in the original ij -coordinate system (a) and in the new kl -coordinate system (b).

Additionally, path a has fewer (i, j) pairs than path b and is therefore likely to have less accumulated alignment error, simply because it is shorter. For this reason, some authors force the optimal path to pass through two specified points, but this requires manual interpretation of the first and last corresponding depths (Le Nir *et al.*, 1998; Wu & Nyland, 1987). This approach was in fact used to compute the optimal path in Figure 2.1b. I performed manual interpretation of two pairs of corresponding depths (805, 845) and (1505, 1545) in logs 1 and 2 and constrained the path to pass through these points.

Alternatively, one might normalize alignment errors along a path by the number of (i, j) pairs in that path. This too is costly, as it requires backtracking along all possible paths to

find the total number of (i, j) pairs in each path.

To address this problem, we compute alignment errors in a rotated kl -coordinate system with

$$\begin{aligned} k = j + i & \quad i = \frac{k-l}{2} \\ l = j - i & \quad j = \frac{k+l}{2} \end{aligned} \iff \quad (2.3)$$

where k indexes depth and l indexes lag, a difference between two depths. In the new kl -coordinate system, alignment errors are now

$$e_{IJ}[k, l] \equiv \left| f \left[\frac{k-l}{2}, I \right] - f \left[\frac{k+l}{2}, J \right] \right|^p, \quad (2.4)$$

for $k = 0, 1, \dots, N_k - 1$, $l = l_{\min}, \dots, l_{\max}$,

where $N_k = 2N_z - 1$, l_{\min} and l_{\max} are specified bounds on lag (depth difference), and p is any positive value. Because i and j must be integers, equation 2.4 implies that alignment errors $e_{IJ}[k, l]$ are calculated only for values of k and l for which $k + l$ (and $k - l$) is even.

In dynamic warping, we now seek a path, a sequence of (k, l) pairs, that minimizes the accumulated alignment errors:

$$D_{IJ} = \min_{\text{path}} \sum_{(k,l) \in \text{path}} e_{IJ}[k, l]. \quad (2.5)$$

Figure 2.2b shows paths a and b on the kl -coordinate system with path a extending into areas where either $f[i, I]$ or $f[j, J]$ is null. Both paths begin at $k = 0$ and end at $k = N_k - 1$, so that accumulated alignment errors for path a will not be less than those for path b , simply because path a is shorter, as in Figure 2.2a. Alignment errors computed for density logs $I = 1$ and $J = 2$ are shown on the kl -coordinate system in Figure 2.3a with the optimal path overlain in Figure 2.3b. This path lies at roughly $l = 40$, implying that depths in log $J = 2$ are about 40 m deeper than corresponding depths in log $I = 1$.

A common approach in well log correlation is to use the L_2 -norm ($p = 2$) in the alignment error calculation (Doveton, 1994; Lineman *et al.*, 1987; Wu & Nyland, 1987). Although the L_2 -norm is sufficient in many applications of dynamic warping, such as for speech recognition

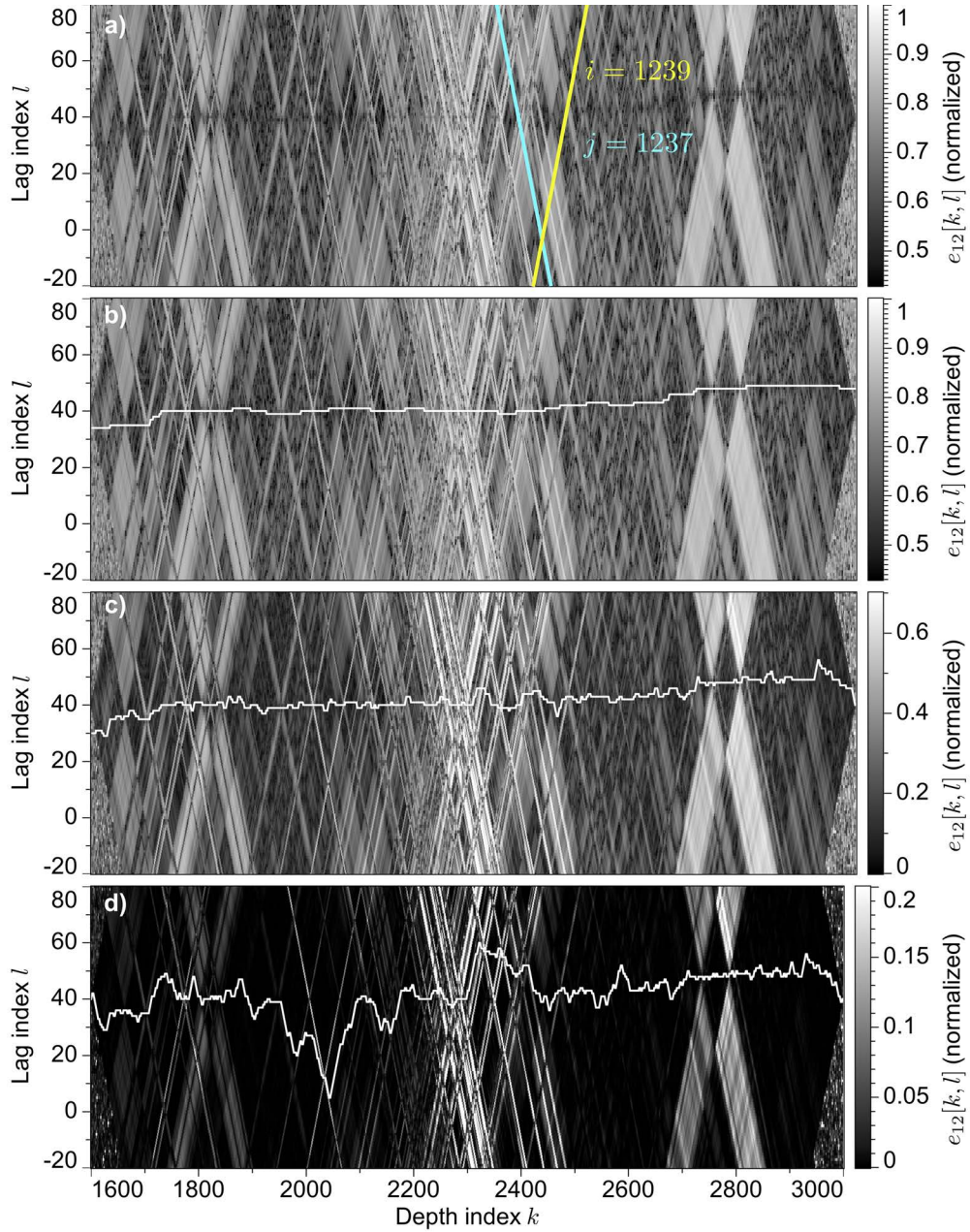


Figure 2.3: Normalized alignment errors for logs $I = 1$ and $J = 2$, computed on the kl -coordinate system (a), where the blue line denotes sample $j = 1237$ and the yellow line denotes sample $i = 1239$. Alignment errors were computed for $p = \frac{1}{8}$ (b), $p = \frac{1}{2}$ (c), and $p = 2$ (d), and their respective optimal paths overlain in white. As p increases, large errors dominate and result in erroneous warping paths.

(Sakoe & Chiba, 1978) or aligning seismograms (Hale, 2013), this norm is often unsuitable for well log correlation because of large measurement errors that are common in well logs. Alignment errors computed between samples with such measurement errors are amplified when $p = 2$ because the L_2 -norm squares the differences between log values. Therefore, these large alignment errors dominate any warping path on which they lie, thereby increasing the accumulated alignment error over such paths immensely. If such large measurement errors lie on the correct path, the accumulated alignment error at the end of that path might not be minimized, resulting in an incorrect correlation.

As the value of p decreases, the alignment error $e_{IJ}[k, l]$ becomes less sensitive to measurement errors. Alignment errors for density logs 1 and 2 computed for various values of p are shown in Figures 2.3b, 2.3c, and 2.3d. These alignment errors are normalized by the maximum alignment error and their respective optimal paths are denoted by the overlaying white curves. Figure 2.3d shows that the optimal path is highly influenced by large measurement errors for large p . We choose $p = \frac{1}{8}$ (the $L_{\frac{1}{8}}$ -norm) as it seems to effectively reduce the influence of such large measurement errors in the Teapot Dome density logs.

2.2 Replacing missing data

In practice, it is common for the optimal path to pass through (i, j) pairs where either $f[i, I]$ or $f[j, J]$ is null, as for path a in Figure 2.2b. When calculating alignment errors, we temporarily replace null values in logs I and J with randomly chosen non-null values from these respective logs. Replacing missing data in this way yields alignment errors comparable to those computed from non-null values.

Suppose, instead, that null values are replaced with zeros. An alignment error $e_{IJ}[k, l]$ calculated for non-null $f[i, I]$ and $f[j, J] = 0$ would then be artificially high. Paths passing through several (i, j) pairs for which either $f[i, I]$ or $f[j, J]$ is null would tend to have relatively large accumulated alignment errors and not be optimal. Alternatively, if both $f[i, I]$ and $f[j, J]$ are null, the alignment error $e_{IJ}[k, l]$ would equal zero, so that the optimal path would tend to pass through the point (i, j) . It is important to note that we do not

compute alignment errors before the beginnings and after the ends of both logs, where both $f[i, I]$ and $f[j, J]$ are null.

2.3 Accumulation and backtracking

From the alignment errors $e_{IJ}[k, l]$, we recursively accumulate alignment errors $d_{IJ}[k, l]$ as follows:

$$d_{IJ}[0, l] = e_{IJ}[0, l] , \quad (2.6)$$

$$d_{IJ}[1, l] = e_{IJ}[1, l] + \min \left\{ \begin{array}{l} d_{IJ}[0, l - 1] \\ d_{IJ}[0, l + 1] \end{array} \right. , \quad (2.7)$$

$$d_{IJ}[k, l] = e_{IJ}[k, l] + \min \left\{ \begin{array}{l} d_{IJ}[k - 1, l - 1] \\ d_{IJ}[k - 2, l] \\ d_{IJ}[k - 1, l + 1] \end{array} \right. , \quad (2.8)$$

for $k = 2, 3, \dots, N_k - 1$.

All lags l in the specified range $[l_{\min}, l_{\max}]$ must be considered in the calculation of accumulated alignment errors $d_{IJ}[k, l]$ because we do not yet know which lags lie on the optimal path. The computational stencil for equation 2.8 is shown in Figure 2.4 for one sample of $d_{IJ}[k, l]$. Like $e_{IJ}[k, l]$, $d_{IJ}[k, l]$ is computed only where $k + l$ (and hence $k - l$) is even.

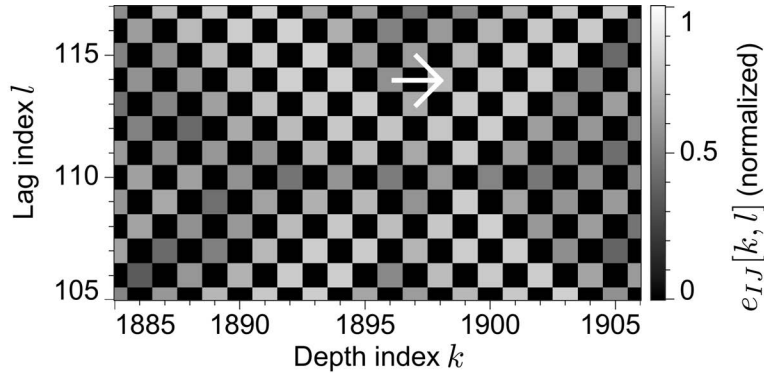


Figure 2.4: New computational stencil on a close up view of alignment errors computed for density logs $I = 1$ and $J = 2$. Alignment errors $e_{IJ}[k, l]$ are computed only where $k + l$ is even.

After accumulation, we scan the accumulated alignment errors $d_{IJ}[k, l]$ at index $k = N_k - 1$ to find the lag index l of the minimum accumulated alignment error D_{IJ} at the end of

the optimal path. From equation 2.8, it is clear that the previous sample on that path must be $(k-1, l-1)$, $(k-2, l)$, or $(k-1, l+1)$, depending upon which of the three accumulated alignment errors is smallest. Similar backtracking is performed to find optimal lags l for every $k = N_k - 1, N_k - 2, \dots, 0$. The resulting optimal sequence of (k, l) pairs represent pairs of corresponding depths.

By warping each of the 78 log pairs (denoted by line segments in Figure 1.2b), we obtain for each log pair a sequence of corresponding depths. Figure 2.5 displays three pairs of density logs before and after pairwise alignment using our modified dynamic warping algorithm. Figures 2.5d, 2.5e, and 2.5f show log values for only the computed corresponding log depths. Although large measurement errors are apparent in log 4, they have little effect on the alignment of the logs in Figure 2.5d.

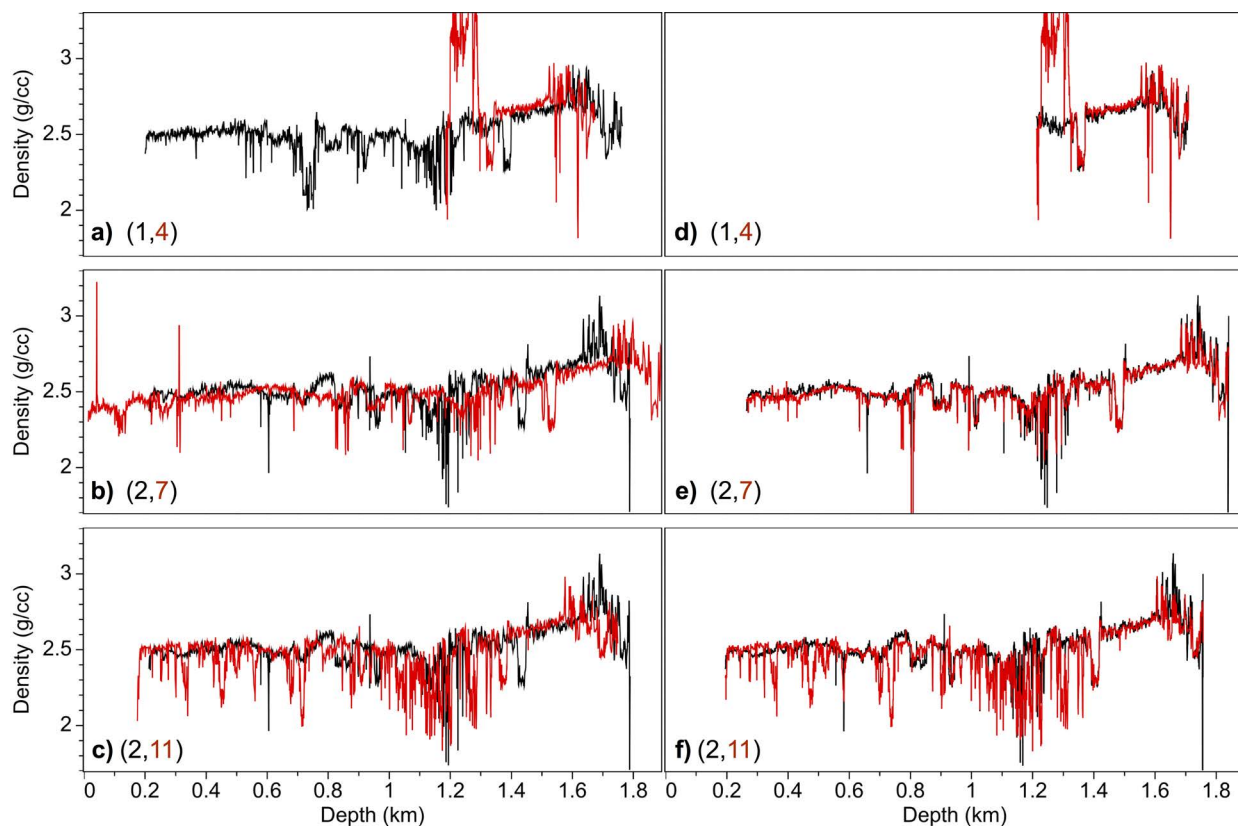


Figure 2.5: Three density log pairs before (a, b, c) and after (d, e, f) warping. Log indices (I, J) are denoted in black and red, corresponding to the colors of the logs.

CHAPTER 3

SIMULTANEOUS MULTI-WELL LOG CORRELATION

A common approach to correlating a set of three or more well logs is to perform pairwise log correlation in some sequence, where each log is correlated to only the log before it in this sequence (Lallier *et al.*, 2014; Le Nir *et al.*, 1998). In such methods, earlier correlations are used as constraints for later ones. Therefore, correlation errors propagate through each successive correlation. This implies that the final solution depends on the chosen sequence of pairwise correlations. For the 13 logs in Figure 1.2, there are over 6 billion ways in which one could order the logs, and thus over 6 billion different solutions. We seek a final correlation that does not depend on any ordering of the logs. In this chapter, I show how to compute such a solution.

Chapter 2 shows how to find an optimal correlation for every log pair in a set of well logs. For the final correlation, we additionally require that these pairwise correlations be consistent for all logs. For example, suppose we choose a depth z_i in log I and find corresponding depths in all other logs. From Figure 3.1 we can see that corresponding depths z_i and z_j in logs I and J are offset by some depth shift s . If we sum depth shifts like this one, for each pair of corresponding depths along any cycle (a distinct, closed path among three or more logs), we expect the sum of all of the shifts to be zero when we return to depth z_i in log I .

Such consistency can be maintained through dynamic warping if additional constraints are introduced, similar to those used to register multicomponent seismic images (Compton & Hale, 2013). For each set of corresponding depths, we would have one constraint per cycle. Recall that for the 13 wells with locations in Figure 1.2a, the number of cycles $N_c \approx 5$ billion and therefore, we would have 5 billion constraints per set of corresponding depths. Moreover, the required array of alignment errors increases in dimension with each additional log. Thus, the computational cost of using dynamic warping to consistently correlate L logs,

each with N_z depths, is $O(N_z^L)$. To put this into perspective, Lallier *et al.* (2014) explain that storing the 12-dimensional array of alignment errors for a correlation with $L = 12$ logs and $N_z = 10$ markers requires 4GB of RAM. Because it is common to correlate tens to hundreds of logs with $N_z \gg 10$ samples, it becomes infeasible to use dynamic warping alone to simultaneously correlate multiple logs. Therefore, an additional method must be used to achieve consistency among pairwise correlations.

In this chapter, I describe how to solve for shifts that optimally align all logs simultaneously, using least-squares. I first explain how to develop such a least-squares problem. Then, I describe how we constrain shifts to prevent unnecessary shifting, stretching, or squeezing of logs. Next, I explain how to apply these shifts to align logs. Finally, I describe the modifications required to extend our simultaneous correlation method to multiple log types.

3.1 Computing shifts

After computing many pairs of corresponding depths, such as the pair illustrated in Figure 3.1, we must find depth shifts $s(z, l)$ for every sample in every log so that all pairs of corresponding depths are consistent. For every depth z in log l , let $\tau(z, l)$ denote a corresponding relative geologic time (RGT) and inversely, let $z(\tau, l)$ denote a corresponding depth for every RGT τ . We can then define the following relationships:

$$\tau(z, l) \equiv z + s(z, l) , \tag{3.1}$$

$$z(\tau, l) \equiv \tau - r(\tau, l) , \tag{3.2}$$

$$s(z, l) \equiv r(\tau(z, l), l) , \tag{3.3}$$

$$r(\tau, l) \equiv s(z(\tau, l), l) , \tag{3.4}$$

where $s(z, l)$ represents the depth shift for log l at depth z and $r(\tau, l)$ represents the RGT shift for log l at RGT τ . Due to thickening and thinning of beds, unconformities, and faulting, it is common for shifts $s(z, l)$ to vary with depth, and shifts $r(\tau, l)$ to vary with RGT. However, if these shifts do not vary with depth or RGT, then $s(z, l) = r(\tau, l)$ for all depths z and RGT τ . If the quantity on the left-hand side of any one of the above equations

is known, we can derive the other three quantities. For example, suppose we know $r(\tau, l)$. We can first use equation 3.2 to solve for $z(\tau, l)$ and then invert $z(\tau, l)$ to get $\tau(z, l)$. Finally, we can compute $s(z, l)$ using equation 3.3.

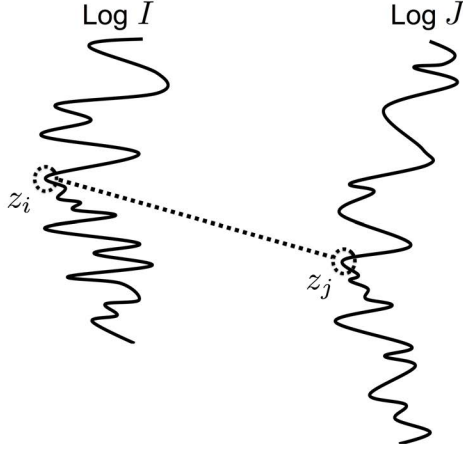


Figure 3.1: Each depth z_i in log I has one or more corresponding depths z_j in log J . For such pairs of depths, log values $f(z_i, I)$ and $f(z_j, J)$ should be similar.

After computing shifts $s(z, l)$ such that all pairs of corresponding depths are consistent, equation 3.1 can be used to compute a time $\tau(z, l)$ for each sampled depth z and thereby find a log value $\tilde{f}(\tau, l)$ for every time τ . Specifically, we can first convert the function $\tau(z, l)$ to $z(\tau, l)$ and then compute $\tilde{f}(\tau, l) = f(z(\tau, l), l)$.

Recall that depths z_i in log I and z_j in log J correspond if they have the same relative geologic time $\tau(z_i, I) = \tau(z_j, J)$ and therefore,

$$z_i + s(z_i, I) = z_j + s(z_j, J) . \quad (3.5)$$

Rearranging equation 3.5 so that corresponding depths are on the right and unknown shifts are on the left, we have

$$s(z_i, I) - s(z_j, J) = z_j - z_i . \quad (3.6)$$

Notice that if we add a constant to all shifts $s(z, l)$, equation 3.6 will still be satisfied and therefore, the solution $s(z, l)$ is non-unique. In fact, this non-uniqueness is even worse than this, but we will discuss later how we constrain the shifts to address this problem.

Every depth in every log will have a corresponding shift, yielding LN_z unknown shifts s . The number N_p of pairs of corresponding depths we can find among all pairs of logs depends on the number of non-null values in the logs, but typically is much greater than the number of shifts. For the 13 density logs in Figure 1.1, we have $N_p = 92,000$ depth-pair equations 3.6 and only $LN_z = 25,000$ unknown shifts. Equation 3.6 gives rise to a system of linear equations with many more equations than unknowns.

Let \mathbf{s} denote depth shifts $s(z, l)$ arranged in an $LN_z \times 1$ vector and \mathbf{d}_z be an $N_p \times 1$ vector of depth differences $z_j - z_i$. Our system of equations then becomes

$$\mathbf{D}_s \mathbf{s} \approx \mathbf{d}_z, \quad (3.7)$$

where \mathbf{D}_s is a sparse $N_p \times LN_z$ matrix operator that computes the differences between shifts in equation 3.6. Each row of the matrix \mathbf{D}_s has only two non-zero elements: a 1 and a -1, corresponding to the difference in shifts $s(z_i, I)$ and $s(z_j, J)$ in equations 3.6.

Because this linear system has far more equations than unknowns, it is unlikely that all equations 3.6 will be satisfied. Therefore, we seek a solution \mathbf{s} that minimizes, in a least-squares sense, the sum of squared differences between the difference in shifts $s(z_i, I) - s(z_j, J)$ and difference in depths $z_j - z_i$ for corresponding depth pairs:

$$\min_{\mathbf{s}} \|\mathbf{D}_s \mathbf{s} - \mathbf{d}_z\|^2. \quad (3.8)$$

Such a solution can be found by solving the normal equations:

$$\mathbf{D}_s^T \mathbf{D}_s \mathbf{s} = \mathbf{D}_s^T \mathbf{d}_z. \quad (3.9)$$

In general, \mathbf{D}_s has a large number of rows and columns. For the 13 Teapot Dome density logs, \mathbf{D}_s is a $92,000 \times 25,000$ matrix. Because of its large size, we never explicitly build the matrix \mathbf{D}_s . Instead, we supply two methods: one that, when applied to vector \mathbf{s} , has the effect of multiplying $\mathbf{D}_s^T \mathbf{D}_s$ and \mathbf{s} and another that directly computes the right-hand side vector $\mathbf{D}_s^T \mathbf{d}_z$.

Because of the large number LN_z of equations in equation 3.9, we require an iterative method, such as the conjugate gradient method (e.g., Shewchuk, 1994), to solve for the

shifts \mathbf{s} . For any system of the form $\mathbf{A}\mathbf{x} = \mathbf{b}$, like equation 3.9, where \mathbf{A} is a matrix, \mathbf{x} is an unknown vector, and \mathbf{b} is a known vector, the conjugate gradient method requires that the matrix \mathbf{A} be symmetric nonnegative-definite (SNND). The matrix $\mathbf{D}_s^T \mathbf{D}_s$ is both symmetric ($\mathbf{D}_s^T \mathbf{D}_s = (\mathbf{D}_s^T \mathbf{D}_s)^T$) and nonnegative-definite ($\mathbf{x}^T \mathbf{D}_s^T \mathbf{D}_s \mathbf{x} = \|\mathbf{D}_s \mathbf{x}\|^2 \geq 0$, for any \mathbf{x}) and therefore, we can use conjugate gradients to solve equation 3.9.

If an estimate of \mathbf{s} is known, the conjugate gradient method allows us to use this estimate as a starting value \mathbf{s}_0 . We have no prior information about shifts \mathbf{s} and therefore assume $\mathbf{s}_0 = \mathbf{0}$. We then update $s(z, l)$ iteratively, stopping the conjugate-gradient (CG) iterations when residuals $\|\mathbf{D}_s^T \mathbf{D}_s \mathbf{s} - \mathbf{D}_s^T \mathbf{d}_z\|^2 < 0.005 \times \|\mathbf{D}_s^T \mathbf{d}_z\|^2$ or when 1000 iterations have been performed, whichever occurs first.

Because subsurface geology typically varies slowly laterally, we expect nearby logs to be more similar than those far apart. For this reason, and to reduce computation time, one might choose to only perform pairwise correlation of logs for wells separated by some distance less than a user-defined upper bound. However, this method is unreliable because the pairwise correlation of two logs for wells separated by a slightly greater distance might significantly improve the final correlation of all logs, but would never be computed.

Alternatively, one might weight equations 3.6 inversely proportional to distances between wells. It is possible, though, for the pairwise correlation of two logs for nearby wells to be unreliable because of measurement errors in one or both logs. With a weight inversely proportional to distance, depth-pair equations 3.6 from such an unreliable correlation would be given high weight and would reduce the accuracy of the final correlation.

Instead, we perform pairwise correlations for all possible log pairs and use the total accumulated alignment error D_{IJ} , computed during pairwise correlation of logs I and J , to derive weights for depth-pair equations 3.6. We weight these equations inversely proportional to the square of the L_p -norm of alignment errors already computed for pairwise optimal paths, so that pairwise correlations with large error (less reliable correlations) are given less weight than those with small error (more reliable correlations). Through experimentation, we found

that the square of the L_p -norm was more effective than the L_p -norm itself. We compute the squared L_p -norm of alignment errors for each pairwise optimal path as $\left(\frac{D_{IJ}}{N_{IJ}}\right)^{2/p}$, where N_{IJ} is the number of corresponding depth pairs.

When a log has few non-null values, its pairwise correlations may be unreliable, because a few non-null values are likely to be only coincidentally correlated with values in another log. For this reason, we give higher weight to pairwise correlations of logs with larger numbers N_{IJ} of corresponding depth pairs. Therefore, we compute weights w_{IJ} for depth-pair equations 3.6 as

$$w_{IJ} = \frac{N_{IJ} \left(\frac{N_{IJ}}{D_{IJ}}\right)^{2/p}}{\sum_{I=1}^L \sum_{J=I+1}^L N_{IJ} \left(\frac{N_{IJ}}{D_{IJ}}\right)^{2/p}}, \quad (3.10)$$

where these weights are normalized to the range $[0, 1]$.

3.2 Removing unnecessary stretching and squeezing

Although we can find depth shifts \mathbf{s} that solve equation 3.9, recall that this solution is not unique because aligned logs, such as those in Figure 3.2a, will remain aligned if all logs are shifted or squeezed or stretched vertically. RGT τ in Figure 3.2b has been replaced with $1.4\tau - 300$, thus squeezing and shifting the logs in Figure 3.2a.

To prevent such unnecessary squeezing or stretching or shifting, we might constrain the average shift over all logs to be zero for all depths. We can implement this constraint by replacing $s(z, l)$ in equation 3.1 with $s(z, l) - \bar{s}(z)$, yielding

$$\tau(z, l) = z + s(z, l) - \bar{s}(z), \quad (3.11)$$

where

$$\bar{s}(z) = \frac{1}{L} \sum_{l=1}^L s(z, l). \quad (3.12)$$

When mapping logs $f(z, l)$ from depth to RGT, this constraint implies that, for every constant depth z , each log sample $f(z, l)$ can be shifted up or down, but the average shift over all logs is zero.

Suppose we have a solution $s(z, l)$. Using equation 3.11, we can find RGTs for depths z_i and z_j in logs I and J , respectively:

$$\tau(z_i, I) = z_i + s(z_i, I) - \bar{s}(z_i) , \quad (3.13)$$

$$\tau(z_j, J) = z_j + s(z_j, J) - \bar{s}(z_j) . \quad (3.14)$$

For z_i and z_j to correspond, they must have the same RGT, $\tau(z_i, I) = \tau(z_j, J)$. Typically, the average shift at depth z_i is not equal to the average shift at depth z_j ; that is, $\bar{s}(z_i) \neq \bar{s}(z_j)$ and therefore, our assumption that corresponding RGTs are equal is no longer satisfied, resulting in misaligned logs.

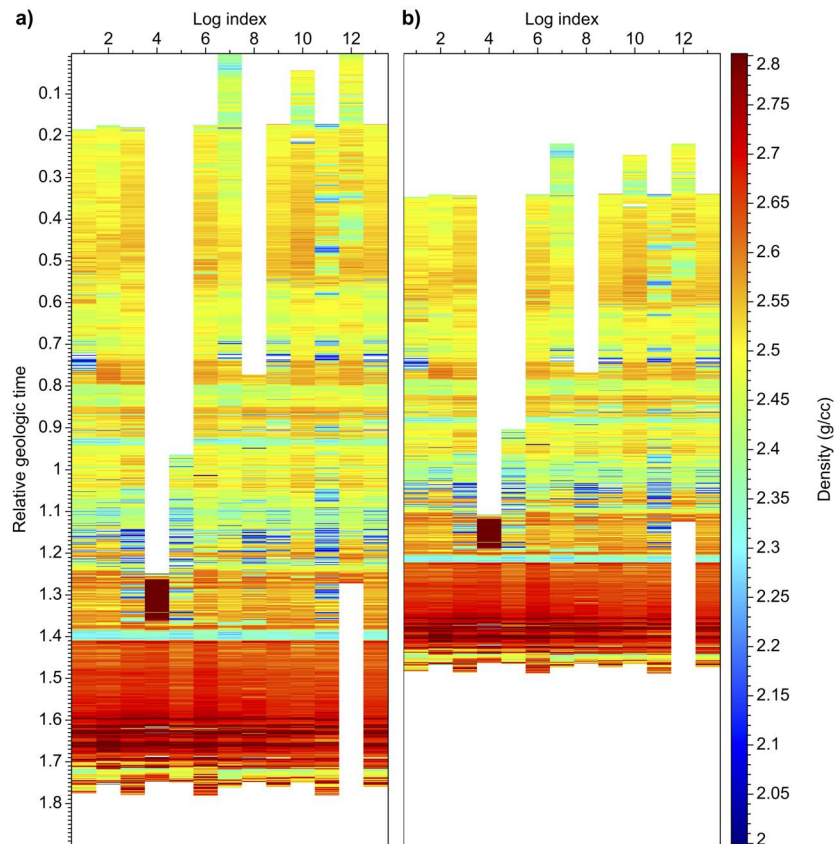


Figure 3.2: Aligned logs (a) remain aligned after being squeezed and shifted (b).

Alternatively, we can use the relationship of $s(z, l)$ and $r(\tau, l)$ in equation 3.3 to rewrite equation 3.1 as

$$\tau(z, l) = z + r(\tau(z, l), l) . \quad (3.15)$$

Now, by replacing $r(\tau, l)$ in equation 3.15 with $r(\tau, l) - \bar{r}(\tau)$, we effectively constrain the average shift over all logs to be zero, for all RGT:

$$\tau(z, l) = z + r(\tau(z, l), l) - \bar{r}(\tau(z, l), l) , \quad (3.16)$$

where

$$\bar{r}(\tau) = \frac{1}{L} \sum_{l=1}^L r(\tau, l) . \quad (3.17)$$

This constraint implies that, for every constant RGT, each log sample $\tilde{f}(\tau, l)$ may have come from a depth above or below, but the average shift over the logs is zero. If all log samples for a constant RGT came from depths above, then this implies unnecessary shifting.

Suppose again that $s(z, l)$ is a solution, where $s(z, l) = r(\tau(z, l), l)$. For depths z_i and z_j , we can use equation 3.16 to find corresponding RGTs:

$$\tau(z_i, I) = z_i + r(\tau(z_i, I), I) - \bar{r}(\tau(z_i, I)) , \quad (3.18)$$

$$\tau(z_j, J) = z_j + r(\tau(z_j, J), J) - \bar{r}(\tau(z_j, J)) . \quad (3.19)$$

If z_i and z_j correspond, then $\tau(z_i, I) = \tau(z_j, J)$ and therefore, $\bar{r}(\tau(z_i, I)) = \bar{r}(\tau(z_j, J))$. By solving for RGT shifts $r(\tau, l)$ instead of depth shifts $s(z, l)$, we are able to remove unnecessary shifting, stretching, or squeezing from our solution, while aligning the logs. We use the relationship between $r(\tau, l)$ and $s(z, l)$ in equation 3.3 to modify depth-pair equations 3.6 accordingly:

$$r(\tau(z_i, I), I) - r(\tau(z_j, J), J) = z_j - z_i . \quad (3.20)$$

We now seek a solution \mathbf{r} to the following normal equations:

$$\mathbf{D}_r^T \mathbf{D}_r \mathbf{r} = \mathbf{D}_r^T \mathbf{d}_z , \quad (3.21)$$

where \mathbf{D}_r is a sparse $N_p \times LN_z$ matrix with two non-zero elements in each row: a 1 and a -1. Whereas the 1's and -1's in \mathbf{D}_s refer to the differences in shifts $s(z_i, I)$ and $s(z_j, J)$ in equations 3.6, the 1's and -1's in \mathbf{D}_r refer to the differences in shifts $r(\tau(z_i, I), I)$ and $r(\tau(z_j, J), J)$ in equations 3.20 and are therefore in locations different from those in \mathbf{D}_s . Moreover, the locations of the non-zero elements in \mathbf{D}_r depend on $\tau(z, l)$, which in turn depends on the solution $r(\tau, l)$. Thus, our system of equations 3.21 is non-linear. Below, we discuss how we handle this non-linearity, by solving for $r(\tau, l)$ iteratively.

Recall that we constrain the average shift over all logs to be zero for all RGT, in order to remove unnecessary shifting, stretching or squeezing. This constraint can be represented by operator

$$\mathbf{B} = \mathbf{I} - \mathbf{E}\mathbf{\Lambda}\mathbf{E}^T, \quad (3.22)$$

where \mathbf{E} is an $LN_z \times N_z$ sparse matrix such that $\mathbf{E}^T = \left[\mathbf{I} \mid \mathbf{I} \mid \dots \mid \mathbf{I} \right]$ and $\mathbf{\Lambda}$ is a diagonal matrix with entries $\Lambda[n, m] = \frac{1}{L}$, for $n = m$, and zeros elsewhere. Because \mathbf{B} is a SNND matrix, we can include this constraint in preconditioning of our system:

$$\mathbf{M}\mathbf{D}_r^T\mathbf{D}_r\mathbf{r} = \mathbf{M}\mathbf{D}_r^T\mathbf{d}_z, \quad (3.23)$$

where $\mathbf{M} = \mathbf{B}\mathbf{C}\mathbf{B}^T$ is the preconditioner. Here, \mathbf{C} is a recursive exponential filter with half-width $\sigma = 100$ samples that smooths over RGT. Because the matrix $\mathbf{D}_r^T\mathbf{D}_r$ acts as a roughening operator, we choose the preconditioner to include smoothing. This preconditioning is equivalent to the model reparameterization described by Harlan (1995). For simplicity, we omit the preconditioner \mathbf{M} in equations below, though we use it in our preconditioned conjugate gradient solver.

For the 13 density logs, Figure 3.3a shows a close-up of functions $z(\tau, l) = \tau - r(\tau, l)$ computed without preconditioning. Rapid change in depth $z(\tau, l)$ for consecutive RGTs (denoted by the red arrow) represents squeezing of the logs, whereas rapid change in τ for consecutive depths (denoted by the blue arrow) represents stretching. If stretching (or squeezing) occurs in all logs for any constant RGT, then this stretching (or squeezing) is

unnecessary. Figure 3.3b shows functions $z(\tau, l)$ for which, on average, there is no stretching or squeezing, because we computed shifts $r(\tau, l)$ using the preconditioner \mathbf{M} described above.

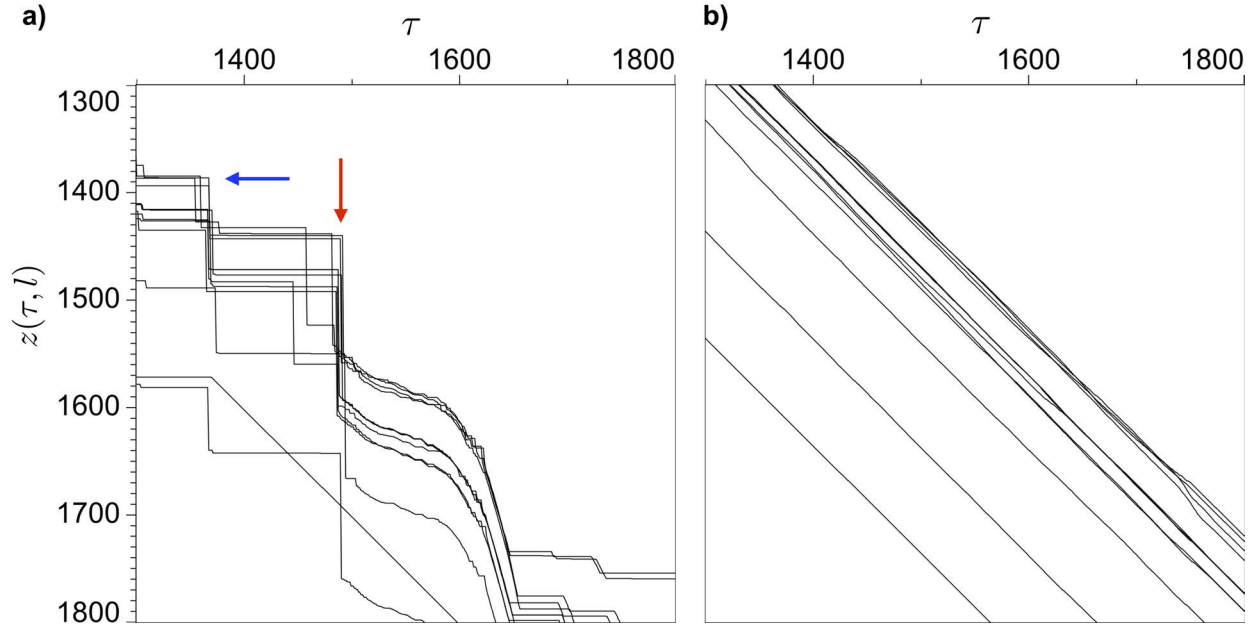


Figure 3.3: A close-up of 13 depth functions $z(\tau, l) = \tau - r(\tau, l)$ (a). Rapid changes in depth for consecutive relative geologic times (red arrow) imply vertical squeezing of the logs and rapid changes in relative geologic time for consecutive depths (blue arrow) imply vertical stretching of the logs. After constraining the average RGT shift over the logs to be zero, each $z(\tau, l)$ is nearly diagonal (b).

3.3 Updating relative geologic time

It is important to note that the function $\tau(z, l)$ is needed to build depth-pair equations 3.20. Also, recall that $\tau(z, l)$ depends on $z(\tau, l)$, which in turn depends on shifts $r(\tau, l)$. To cope with this non-linearity, we update $r(\tau, l)$ and $\tau(z, l)$ iteratively. Because we expect RGT to increase with depth, we begin with simple solutions $r_0(\tau, l) = 0$ and $\tau_0(z, l) = z$. We then use the initial solution $\tau_0(z, l)$ to build the system of equations 3.21, which we then solve using preconditioned conjugate gradients for shifts $r_1(\tau, l)$. We repeat this process to obtain $r_k(\tau, l)$. For each k , we use equation 3.2 to compute depths $z_k(\tau, l) = \tau - r_k(\tau, l)$, and inverse interpolation to get $\tau_k(z, l)$.

Inverse interpolation of $z_k(\tau, l)$ requires that this function be monotonically increasing, that $z_k(\tau_i, l) > z_k(\tau_{i-1}, l)$, implying that $r_k(\tau_i, l) - r_k(\tau_{i-1}, l) < \tau_i - \tau_{i-1} = \Delta\tau$. Because this constraint cannot be easily applied in the conjugate gradient method, we modify shifts $r_k(\tau, l)$ after conjugate-gradient iterations are complete. This modification is performed as follows:

for $i = 1, 2, 3, \dots$

$$\begin{aligned} &\text{if } r(\tau_i, l) \geq r(\tau_{i-1}, l) + \Delta\tau \\ &\quad r(\tau_i, l) = r(\tau_{i-1}, l) + (1 - \epsilon)\Delta\tau, \end{aligned}$$

for some small $\epsilon \ll 1$. We use $\epsilon = 0.001$.

We then iteratively use $\tau_k(z, l)$ and corresponding shifts $r_k(\tau_k(z, l), l)$ as starting values in preconditioned conjugate gradients in order to solve for more accurate shifts $r_{k+1}(\tau, l)$. We refer to the process of using shifts $r_k(\tau, l)$ to update $\tau_k(z, l)$ as *outer iteration k*. Within each of five outer iterations k , we perform $200 \times k$ CG iterations.

3.4 Reparameterization of shifts

Within one oilfield, well logs often appear to be statically shifted versions of one another. In other words, shifts $r(\tau, l)$ are primarily comprised of a large static (RGT independent) shift $c(l)$, plus smaller perturbations $q(\tau, l)$ that represent time-varying shifts (i.e., stretching and squeezing):

$$r(\tau, l) = c(l) + q(\tau, l) . \tag{3.24}$$

If shifts do not vary with RGT, then $r(\tau, l) = c(l) = s(z, l)$. Because time-varying shifts $q(\tau, l)$ are often smaller than static shifts $c(l)$, we can reduce computation time by first solving for $c(l)$ and then computing $q(\tau, l)$.

To solve for static shifts $c(l)$, we use the relationships of corresponding depth pairs (equation 3.20), but now with shifts $c(l)$ that do not vary with RGT:

$$c(I) - c(J) = z_j - z_i . \tag{3.25}$$

Although we have the same number N_p of equations 3.25 as depth-pair equations 3.20, we must find only one shift $c(l)$ for each of L logs, where $N_p \gg L$. With many more equations than unknowns shifts, we again have an overdetermined system of equations:

$$\mathbf{D}_c \mathbf{c} \approx \mathbf{d}_c , \quad (3.26)$$

where \mathbf{D}_c is a $(N_p + 1) \times L$ matrix. Let $D_c[n, m]$ denote the element in the n^{th} row and m^{th} column of \mathbf{D}_c . Then, \mathbf{D}_c has entries

$$D_c[n, m] = \sum_{i=N_z \times (m-1) + 1}^{N_z \times m} D_r[n, i] , \quad (3.27)$$

$$D_c[N_p + 1, m] = 1 , \quad (3.28)$$

for $n = 1, \dots, N_p$ and $m = 1, \dots, L$,

and \mathbf{d}_c is a $(N_p + 1) \times 1$ vector with entries

$$d_c[n] = d_z[n] , \quad (3.29)$$

$$d_c[N_p + 1] = 0 , \quad (3.30)$$

for $n = 1, \dots, N_p$.

The last rows of \mathbf{D}_c and \mathbf{d}_c constrain the average static shift to be zero and thereby eliminates any unnecessary shifting.

Typically, one correlates tens to hundreds of well logs. Because the number of logs L is therefore relatively small, the cost for storing the matrix \mathbf{D}_c in memory is low. For the $L = 13$ density logs in Figure 3.4a, \mathbf{D}_c is a $92,001 \times 13$ matrix. If \mathbf{D}_c were too large to store in memory, we could instead build $L \times L$ matrix $\mathbf{D}_c^T \mathbf{D}_c$ and solve for \mathbf{c} using the normal equations:

$$\mathbf{D}_c^T \mathbf{D}_c \mathbf{c} = \mathbf{D}_c^T \mathbf{d}_c . \quad (3.31)$$

Although $\mathbf{D}_c^T \mathbf{D}_c$ is a much smaller matrix than \mathbf{D}_c , we solve equation 3.26 using QR decomposition because $\mathbf{D}_c^T \mathbf{D}_c$ is less well-conditioned than \mathbf{D}_c .

After applying only static shifts $c(l)$, the 13 density logs in Figure 3.4a are nearly aligned (Figure 3.4b). However, static shifts alone cannot well align these logs. For example, after applying only static shifts (Figure 3.4b), density layers in log 2 near $\tau = 0.8$ are shallower than corresponding layers in log 3 (near $\tau = 0.84$). However, around $\tau = 1.4$, the opposite is true; density layers in log 2 are deeper than corresponding layers in log 3. To correctly align these layers, stretching and squeezing are required.

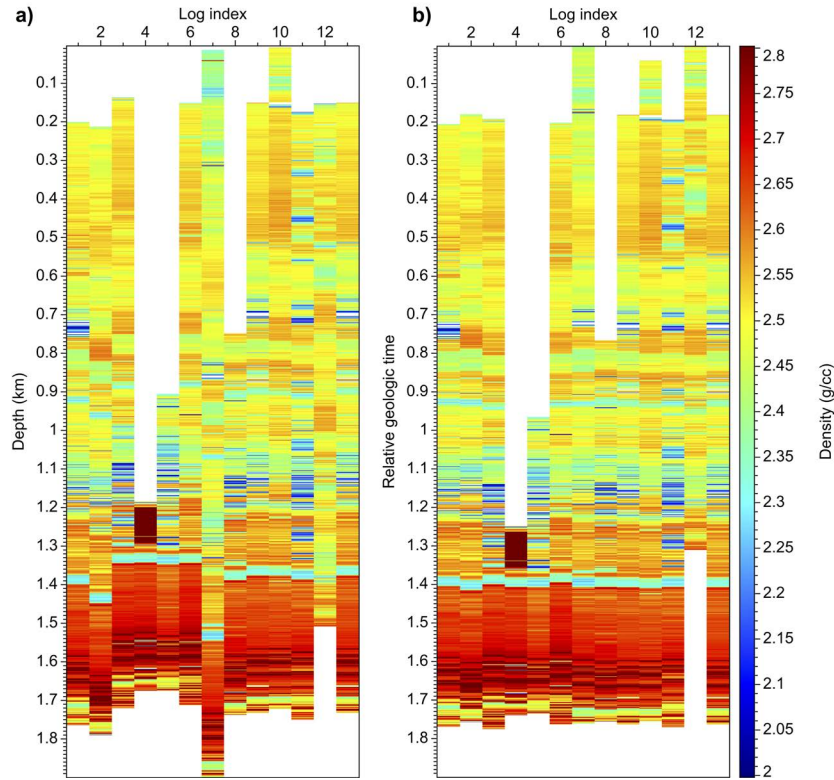


Figure 3.4: 13 Teapot Dome density logs (a) aligned using only static shifts (b).

After computing least-squares best static shifts $c(l)$, we must solve for only small perturbations $q(\tau, l)$. Substituting equation 3.24 into equation 3.20, our depth-pair equations become

$$q(\tau(z_i, I), I) + c(I) - q(\tau(z_j, J), J) - c(J) = z_j - z_i . \quad (3.32)$$

Rearranging equation 3.32 so that the now known static shifts are on the right, we have

$$q(\tau(z_i, I), I) - q(\tau(z_j, J), J) = z_j - z_i + c(J) - c(I) . \quad (3.33)$$

Thus, we have the following non-linear system of equations:

$$\mathbf{D}_r \mathbf{q} \approx \mathbf{d}_u , \quad (3.34)$$

where \mathbf{d}_u is an $N_p \times 1$ vector comprised of the sums of depth differences $z_j - z_i$ and static-shift differences $c(J) - c(I)$. To find the least-squares solution to equation 3.34, we solve the following normal equations using preconditioned conjugate gradients:

$$\mathbf{D}_r^T \mathbf{D}_r \mathbf{q} = \mathbf{D}_r^T \mathbf{d}_u . \quad (3.35)$$

After solving for $q_k(\tau, l)$, within each outer iteration k , we must convert $q_k(\tau, l)$ to $r_k(\tau, l)$ using equation 3.24 and update $\tau_k(z, l)$ as described in Section 3.3. Because most of the solution $r(\tau, l)$ is found using non-iterative QR decomposition and only smaller perturbations $q(\tau, l)$ are found using the iterative conjugate gradient method, the computational cost of computing shifts $r(\tau, l)$ is reduced.

3.5 Missing data

It is likely that some depths in a well log will not correspond to any depths in any other log. Most commonly, this occurs where we have missing data (i.e., null log values), though it can also occur due to unconformities, faults, or changes in bed thickness. Some depths will not appear in any depth-pair equations 3.20, leaving shifts $r(\tau, l)$ for some RGT τ unconstrained. Therefore, we seek to minimize changes in shifts for these RGT. We penalize unnecessary shift changes in the gaps by modifying our system of equations as follows:

$$(\mathbf{D}_r^T \mathbf{D}_r + \xi^2 \mathbf{D}_t^T \mathbf{D}_t) \mathbf{r} = \mathbf{D}_r^T \mathbf{d}_z , \quad (3.36)$$

where \mathbf{D}_t is a finite difference approximation of a time derivative,

$$\xi = \begin{cases} w_p, & \alpha(\tau, l) = 0 \\ 0, & \text{otherwise} \end{cases} , \quad (3.37)$$

w_p is a user-defined weight, and each $\alpha(\tau, l)$ denotes the number of times that $r(\tau, l)$ appears in a depth-pair equation 3.20. Some $r(\tau, l)$ appear in no such equations. Therefore, where

$\alpha(\tau, l) = 0$, we must create additional equations to constrain the corresponding $r(\tau, l)$. The penalty term in equation 3.36 minimizes the time derivative of shifts at RGT where we have no corresponding depths ($\alpha(\tau, l) = 0$), thereby performing constant extrapolation of shifts above the first and below the last non-null sample in each log. For any samples missing within each log, this constraint performs linear interpolation of shifts.

The weight w_p for this penalty term should be comparable to weights w_{IJ} for equations 3.20, which are normalized to the range $[0, 1]$. Therefore, to ensure that this penalty term is satisfied exactly for samples with no corresponding depths ($\alpha(\tau, l) = 0$), we use $w_p = 400$, thereby weighting the penalty term 400 times as much as equations 3.20. Through experimentation, we found that weight $w_p = 400$ yields the best alignment of the 13 Teapot Dome density logs in Figure 3.4a, as well as the Teapot Dome velocity and porosity logs. However, alignments computed for w_p in the range $[300, 900]$ were of similar quality. This broad range, and our normalization of weights w_{IJ} for equations 3.20, suggest that $w_p = 400$ may be a suitable first guess when working with other collections of logs.

3.6 Analyzing log correlations

After computing shifts $r(\tau, l)$ as described above, equation 3.2 can be used to compute a depth $z(\tau, l)$ for each RGT τ and thereby find a log value $\tilde{f}(\tau, l) = f(z(\tau, l), l)$ for every RGT τ . Figure 3.5a shows density logs $f(z, l)$ for $l = 1, 2, \dots, 13$; and Figure 3.5b shows the same logs $\tilde{f}(\tau, l)$ after alignment. Relative ages of sediments among wells can be determined by aligning well logs as shown in Figure 3.5b, where sediments with greater RGT were deposited before those with lesser RGT. The process of determining the relative ages of sediments is called chronostratigraphy and is commonly done by correlating sediments from unusual events, such as ash from volcanic eruptions or tsunami deposits. Typically, beds from such unusual events are relatively thin. Figure 3.5c shows that our automatic and simultaneous log correlation method aligns thin layers consistently among all logs, and therefore can be used in chronostratigraphy to correlate such unusual events.

We can analyze the alignment in Figure 3.5b using several robust statistics. For each constant RGT τ in Figure 3.5, we have a set of corresponding depths that coincides with a geologic horizon. Because we expect similar log values among corresponding depths, we compute, for each RGT, the median density over the logs (Figure 3.6b) and subtract this median from each log sample (Figure 3.6a) to get an absolute deviation (Figure 3.6c). We use the median because it is a robust statistic that is unaffected by large measurement errors common in well logs. For every RGT, we now have a median density and absolute deviations that can be used as robust alternatives to mean and variance in geostatistical simulations.

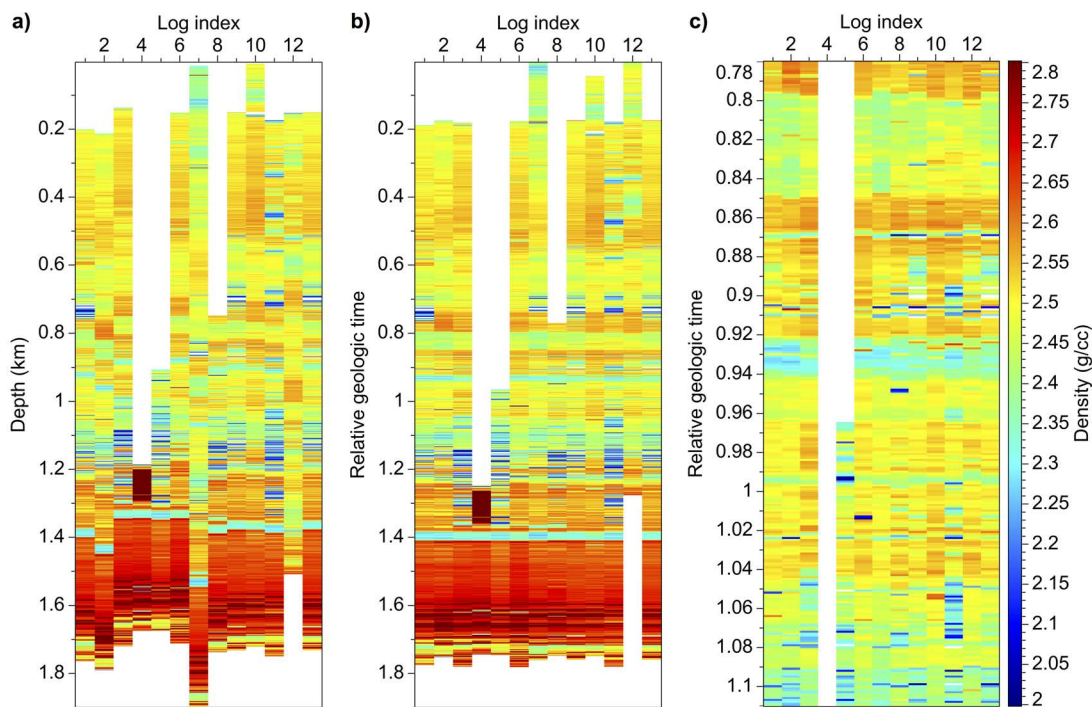


Figure 3.5: 13 Teapot Dome density logs before (a) and after (b) automatic simultaneous correlation. A close-up of aligned density layers between RGT $\tau = 0.78 - 1.2$ (c) shows that thin density layers are aligned consistently among the logs.

High absolute deviations for any log sample can be attributed to several factors, including variation in lithology, unconformities, large measurement errors, as well as misalignment. For the 13 density logs $\tilde{f}(\tau, l)$ in Figure 3.6a, high deviations are primarily found for RGT between $\tau = 1.15 - 1.21$. These high deviations are likely caused by the large amount of

variation in density values among the logs at these RGTs.

To assess the overall quality of alignment, we compute the median absolute deviation (MAD) for an alignment as follows:

$$\text{MAD} = \text{median}_{\tau, l} (|\tilde{f}(\tau, l) - \text{median}_l(\tilde{f}(\tau, l))|) . \quad (3.38)$$

This robust statistic can be used to help select method parameters, such as the value of p in alignment error equation 2.4. For a small subset of logs, one might perform simultaneous multiple log correlation for various parameter values and compute the MADs for the resulting alignments. For simultaneous correlation of all logs, one might then use the parameter values that minimize the MAD for the subset.

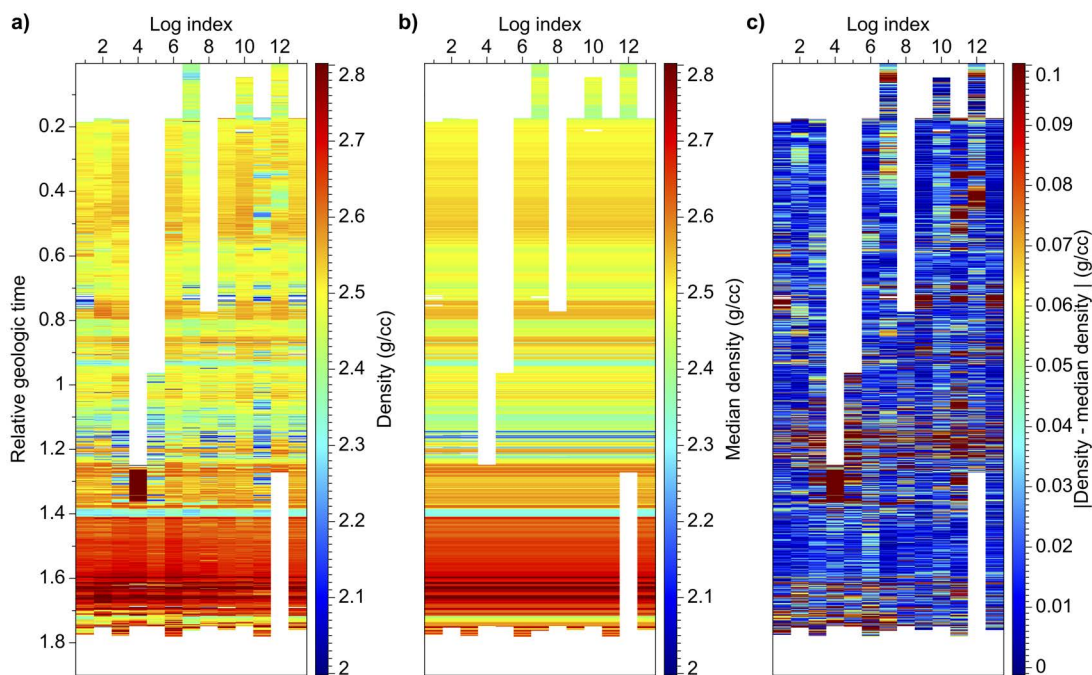


Figure 3.6: For each RGT, absolute deviation (c) is computed by subtracting the median density (b) from the aligned logs (a). High absolute deviations may indicate areas of less reliable correlations.

As an example, we performed simultaneous correlation of the 13 density logs in Figure 3.5a using various L_p -norms in alignment error equation 2.4. The MADs for the resulting different alignments are listed in Table 3.1. Notice that as p increases, MAD increases be-

cause these 13 density logs contain large measurement errors, thereby resulting in erroneous corresponding depth pairs. Because $p = \frac{1}{8}$ minimizes the median absolute deviation for the alignment of these 13 density logs, we use the $L_{\frac{1}{8}}$ -norm when simultaneously correlating these density logs.

Table 3.1: Median absolute deviation (MAD) for different alignments of the 13 density logs in Figure 3.5a, computed using various L_p -norms in alignment error equation 2.4.

norm p	1/16	1/8	1/4	1/2	1	2
MAD of density (g/cc)	0.0205	0.0193	0.0195	0.0235	0.0269	0.0338

3.7 Multiple log types

In well logging, different rock properties are measured. Therefore, it is common to have several logs of various types, though not every well will have all types. For the Teapot Dome example, we have 13 density logs, 11 porosity logs, and 5 velocity logs among the $W = 13$ wells (Figure 3.7).

Fortunately, simultaneous correlation of multiple log types requires only a few minor modifications to the method described above for a single log type. Recall that we begin by performing pairwise correlations in order to find sequences of corresponding depths for every log pair. We do the same when correlating multiple log types, though we now have $\sum_{m=1}^{N_m} \frac{L_m(L_m-1)}{2}$ log pairs, where L_m is the number of logs for log type m and N_m is the number of log types. For the logs in Figure 3.7, we have $\frac{13(13-1)}{2} + \frac{11(11-1)}{2} + \frac{5(5-1)}{2} = 143$ log pairs. It is important to note that, in pairwise correlation, logs of type m are only correlated with logs of the same type.

For each log type m , the first step in pairwise correlation is to compute alignment errors for each sample $f_m[\frac{k-l}{2}, I]$ of log I and each sample $f_m[\frac{k+l}{2}, J]$ of log J (equation 2.4). Recall that as we change the value p of L_p -norm in equation 2.4, the pairwise alignment of two logs changes and therefore, we find a value p that minimizes the MAD for the simultaneous multiple log alignment. It is likely that chosen p for one log type is not best for all other

types and therefore, for each log type m , we first determine value p_m that minimizes the MAD for the simultaneous alignment of the logs. Then, we compute alignment errors for log type m as follows:

$$e_{IJ,m}[k, l] \equiv \left| f_m \left[\frac{k-l}{2}, I \right] - f_m \left[\frac{k+l}{2}, J \right] \right|^{p_m}, \quad (3.39)$$

for $k = 0, 1, \dots, N_k - 1$, $l = l_{min}, \dots, l_{max}$,

where $N_k = 2N_z - 1$ and l_{min} and l_{max} are specified bounds on lag. As for a single log type, we then use these alignment errors to find an optimal sequence of corresponding depths.

After computing sequences of corresponding depths for every log pair, we use these depth pairs to construct equations 3.20. Recall that the number of such equations depends on the number of non-null samples in the logs. Suppose all log types have the same number of non-null samples and therefore the same number N_p of equations. For N_m log types, we would have $N_m \times N_p$ equations. Although the number of log types for each well may vary, each well w has only one sequence of shifts $r(\tau, w)$, yielding $N_z \times W$ unknown shifts, where W is the number of wells. Once again, the number of equations is typically much larger than the number of unknown shifts, and we solve equation 3.36 for shifts \mathbf{r} as described above for a single log type.

There are many factors that suggest we should assign relative weights to depth-pair equations 3.20 that depend on log type. For example, some log types, such as gamma ray, may be better indicators of lithology than others, such as velocity (Looff, 2001). Also, some types, such as gamma ray logs, are highly sensitive to borehole diameter (Looff, 2001) and therefore, prone to measurement errors. For these reasons, we may wish to specify weights w_m for each log type. When building the normal equations 3.21, we now weight each equation proportional to the product of the user-defined weight w_m and the weight $\tilde{w}_{IJ,m}$ for log pair (I, J) of log type m , where

$$\tilde{w}_{IJ,m} = \frac{N_{IJ,m} \left(\frac{N_{IJ,m}}{D_{IJ,m}} \right)^{2/p_m}}{\sum_{I=1}^L \sum_{J=I+1}^L N_{IJ,m} \left(\frac{N_{IJ,m}}{D_{IJ,m}} \right)^{2/p_m}}. \quad (3.40)$$

For log type m , $D_{IJ,m}$ is the total accumulated alignment error, computed using the L_{p_m} -norm, for log pair (I, J) and $N_{IJ,m}$ is the number of corresponding depths. The weight $w_{IJ,m}$ for each depth pair equation 3.20 is

$$w_{IJ,m} = w_m \tilde{w}_{IJ,m} . \quad (3.41)$$

For the simultaneous alignment of density, porosity, and velocity logs in Figure 3.7, we used $p_m = \frac{1}{8}, \frac{1}{4}, \frac{1}{4}$, respectively, in equation 3.39 and for demonstration purposes, we arbitrarily gave depth-pair equations 3.20 for density logs twice as much weight as we did for porosity or velocity logs. By subtracting median density, porosity, and velocity for each RGT (Figure 3.8) from log values in the respective alignments (Figure 3.7), we compute the absolute deviations shown in Figure 3.9. High absolute deviations for most or all RGT in a single well log, such as for porosity logs 2 and 8, can indicate a problem, such as sonde miscalibration, during acquisition of that log.

Plotting MAD as a function of RGT (Figure 3.10) allows us to better determine which RGTs have the most variation in log value. Among all three log types, high absolute deviations are primarily found for RGT between $\tau = 1.15 - 1.23$. Because these high deviations occur over the same interval in all log types, they likely indicate a unit in geologic time with many geologic variations.

We can use our estimated $z(\tau, l)$ to find correlations for every sample in every log by mapping sets of corresponding depths for constant RGT in Figure 3.7 from RGT τ to depth z . Three such correlations are overlain on the cross section of density logs in Figure 3.11a, with location of the cross section denoted by line segments in Figure 3.11b. By comparing density and porosity values for these layers to those identified in formations within Teapot Dome (Beyer & Clutson, 1978) and using the field's stratigraphic column (Figure 3.12), I interpreted these correlations to be the tops of three formations: First Wall Creek, Crow Mountain, and Tensleep.

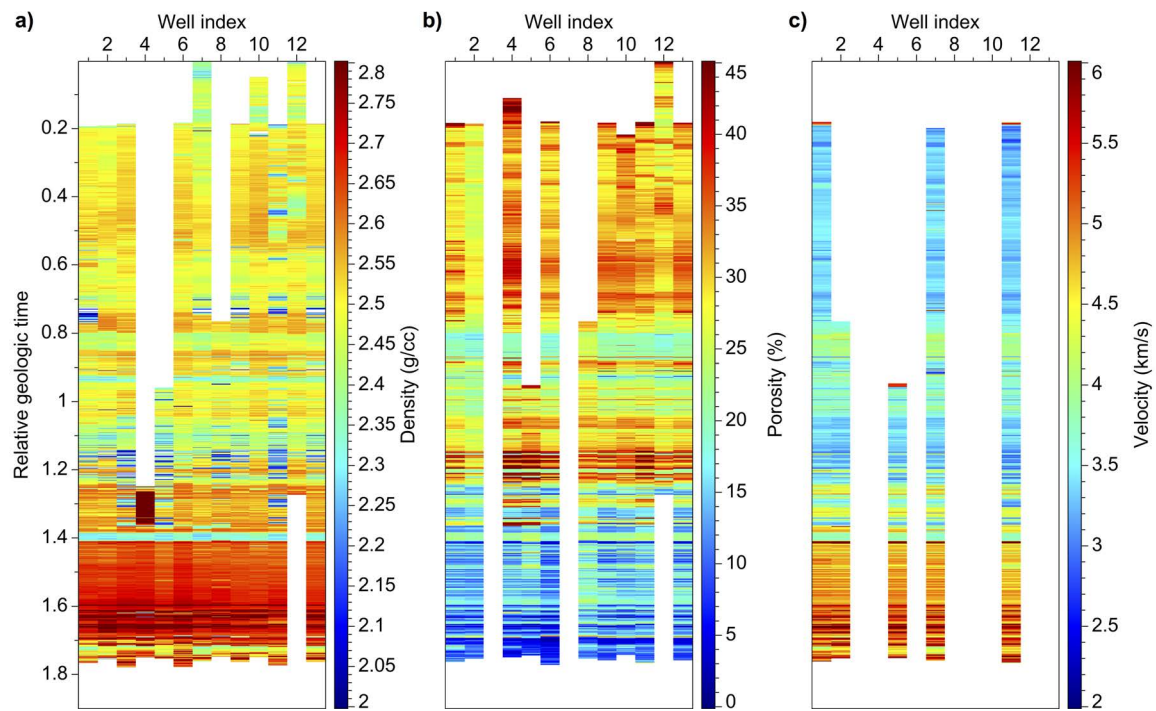


Figure 3.7: 13 density (a), 11 porosity (b), and 5 velocity (c) logs after simultaneous correlation of all three log types.

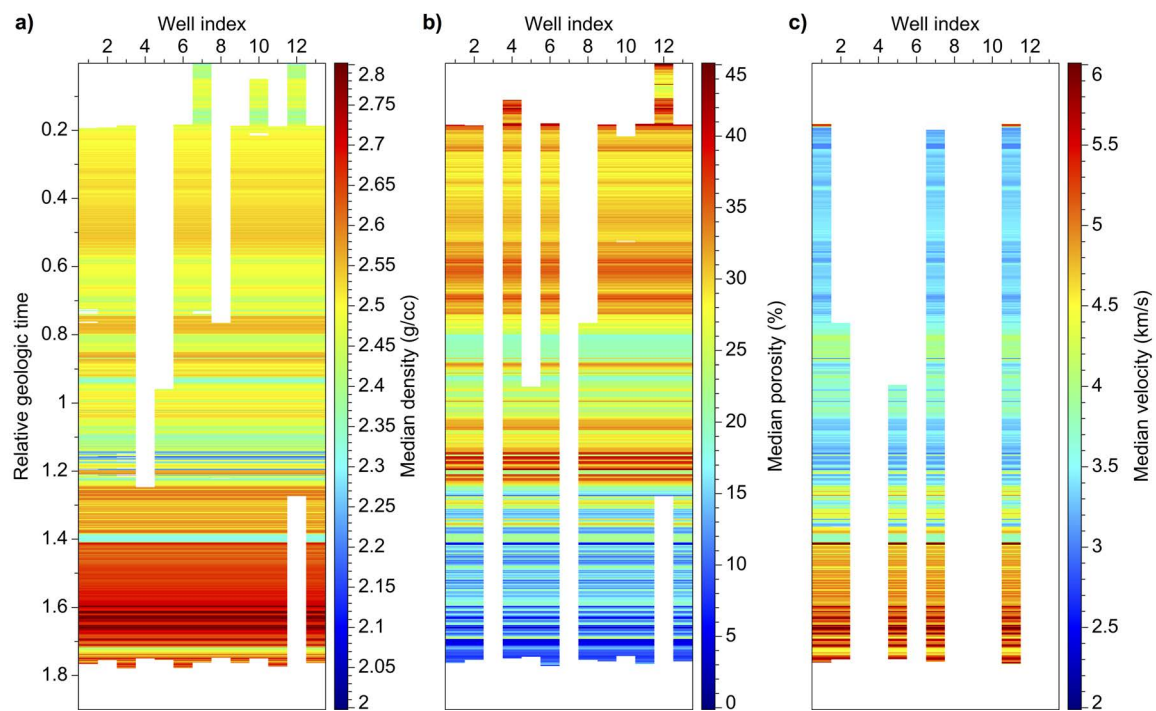


Figure 3.8: Median density (a), porosity (b), and velocity (c) as functions of RGT.

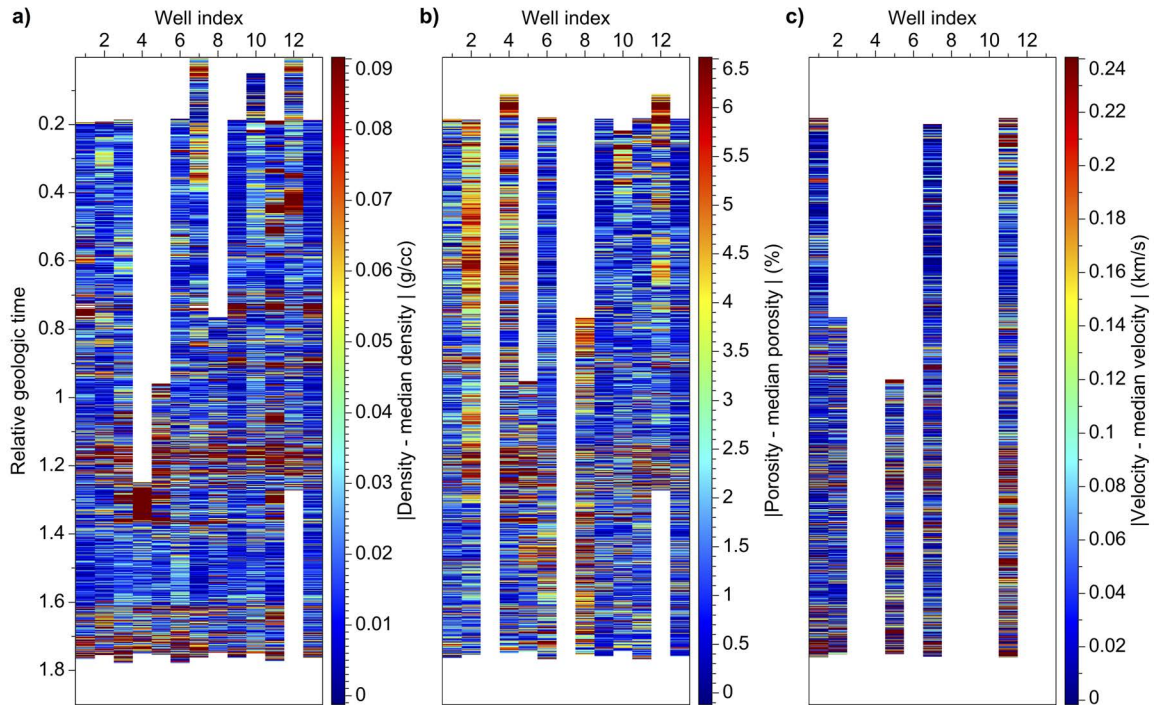


Figure 3.9: Absolute deviation of density (a), porosity (b), and velocity (c).

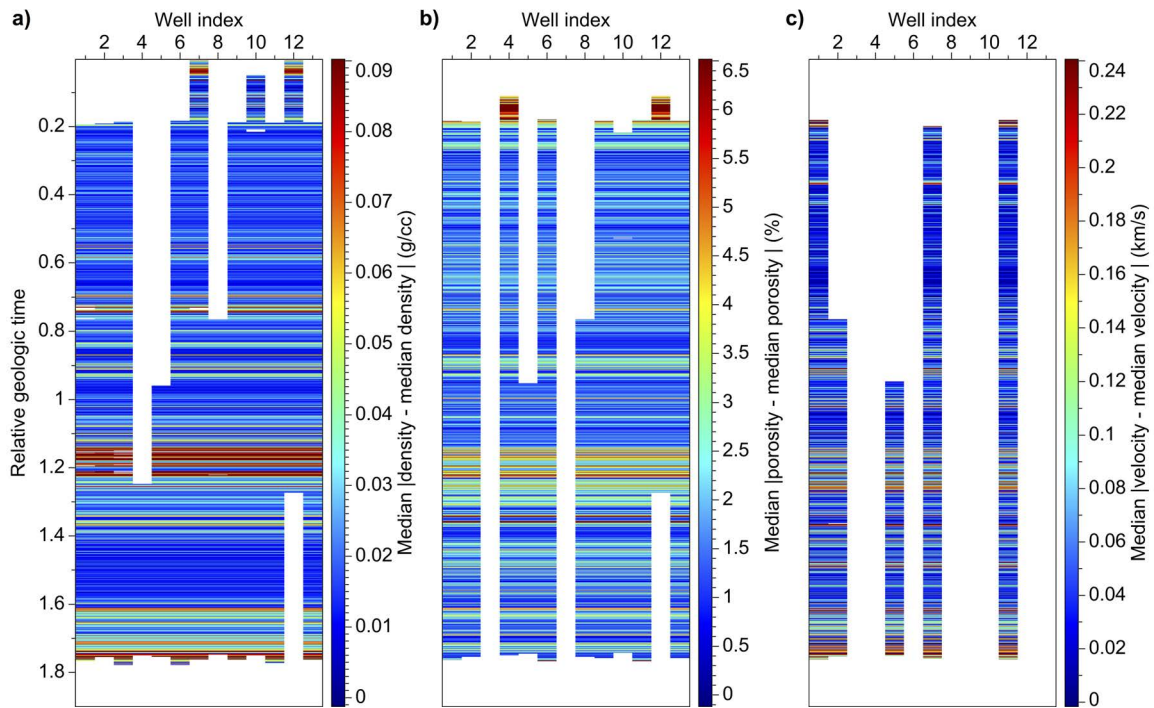


Figure 3.10: Median absolute deviation of density (a), porosity (b), and velocity (c) as functions of RGT.

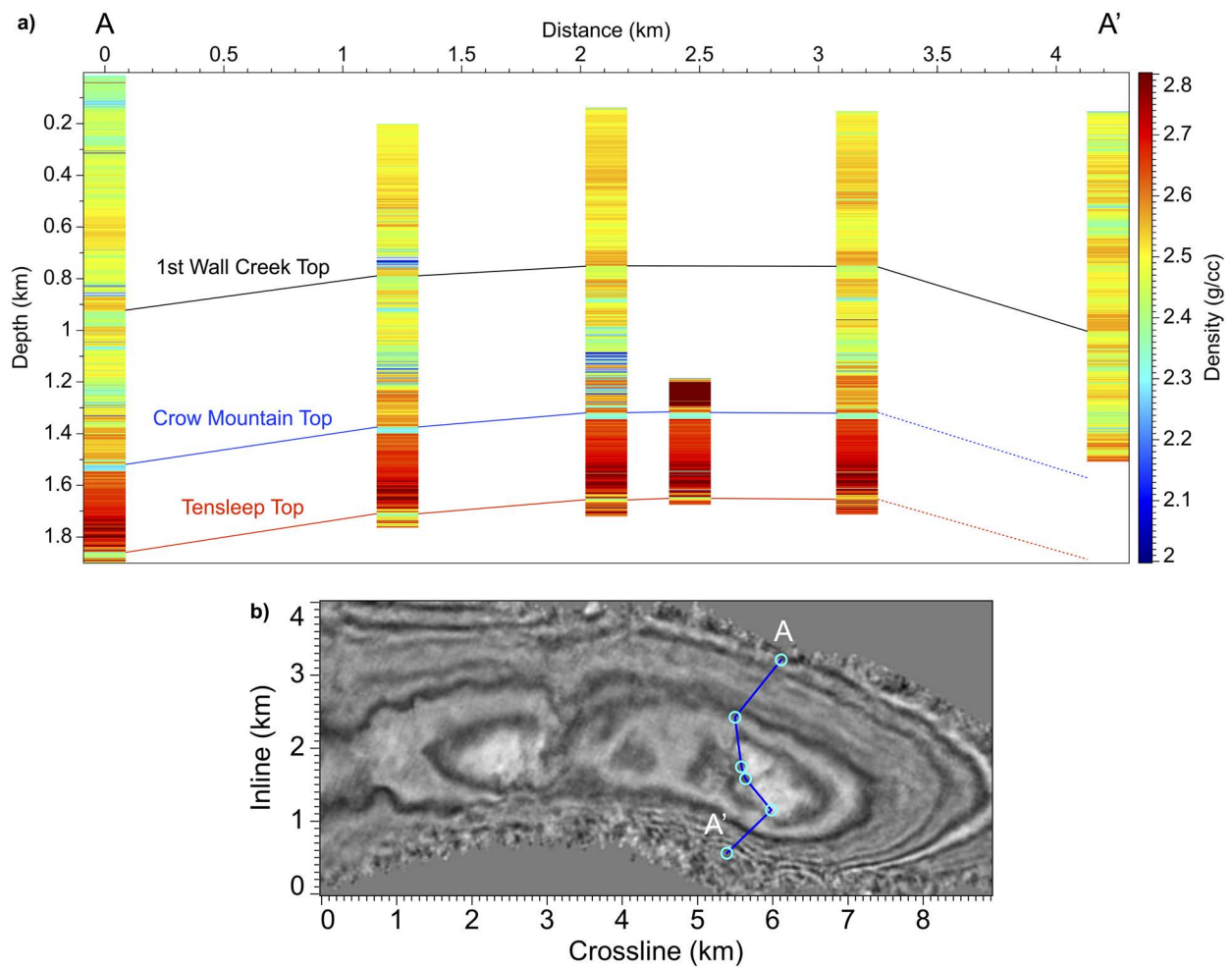


Figure 3.11: Cross section (a) of six Teapot Dome density logs with interpretation of three sets of corresponding depths, found during simultaneous correlation of density, porosity, and velocity logs. Location of the cross section is denoted by line segments (b) overlain on a constant-time slice (at one second) of a corresponding 3D seismic image. The cross section runs from A to A', passing through the apex of the anticline.

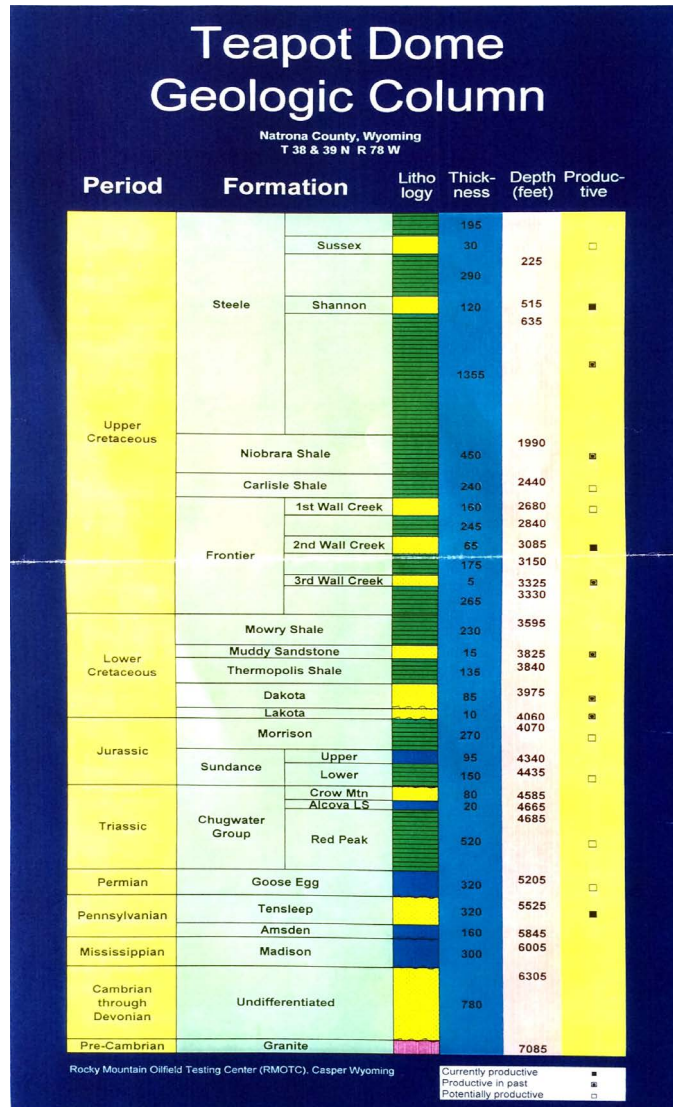


Figure 3.12: Stratigraphic column for Teapot Dome field provided by Rocky Mountain Oilfield Test Center. Green lithologies represent shale, blue represent limestone, yellow represent sandstone-dominated intervals, and pink represent basement rock.

CHAPTER 4

CONCLUSIONS

In this thesis, I presented a two-step method for automatic and simultaneous correlation of multiple well logs. We first find for each log pair a sequence of corresponding depths using our modified dynamic warping algorithm. Our procedure for pairwise log correlation is similar to existing automatic well log correlation methods, but differs primarily in the calculation of alignment errors. In dynamic warping, alignment errors are computed as the L_p -norm of the difference of two log values. It is typical in well log correlation to use $p = 2$, thereby squaring this difference between log values. When large measurement errors are present, alignment errors computed from highly erroneous log values may dominate any warping path they lie on. If such values happen to lie on the correct path, the accumulated alignment error at the end of the path might not be minimized. Thus, the correct path might not be the minimum path. To reduce the effect of large measurement errors, we use an L_p -norm with $p < 2$. Additionally, we compute alignment errors in a transformed coordinate system to ensure that all possible warping paths have equal length, so that the total accumulated alignment error along a path will not be minimized solely due to its short length. At the end of this first step, we've done nothing yet to guarantee consistency of pairwise correlations among all wells.

Using a least-squares method, we then compute shifts, comprised of both static and time-varying shifts, for every sample in every log, that minimize inconsistency among all pairs of corresponding depths. Because aligned logs will remain aligned if shifted, stretched, or squeezed vertically, we constrain the average shift over the logs to be zero, and thereby remove any unnecessary shifting, stretching, or squeezing. By applying these shifts, we find relative geologic times for every log depth, and thereby map all well logs from depth to relative geologic time. For any constant RGT, we can then find a set of corresponding

depths to obtain a final correlation of all logs. Our method is easily extended to multiple log types with the addition of user-defined weights for each type. Using examples from Teapot Dome, we have shown that our method yields consistent correlations and is robust in the presence of large measurement errors frequently found in well logs.

4.1 Future work

In the current implementation of our simultaneous multiple log correlation method, one must specify the maximum possible shift. This maximum shift is used to define bounds l_{min} and l_{max} in the alignment error calculation. In many cases, the maximum shift between two logs increases as the lateral distance between wells increases, due to variation in geologic structures. This is especially true in oilfields, such as Teapot Dome, with structural folding. Specifying a larger maximum shift for all pairwise correlations increases the likelihood of errors in these correlations. Future implementations of our method might instead permit specification of a maximum strain (change in shift over lateral distance).

While computing RGT shifts through a series of outer iterations, we also update relative geologic times $\tau(z, l)$. This is done by first computing depths $z(\tau, l)$ from shifts $r(\tau, l)$, and then inverting to get RGT $\tau(z, l)$. For $z(\tau, l)$ to be invertible, this function must be monotonic, implying that the time derivative of the shifts must be less than one. Because we cannot easily apply such a constraint in the conjugate gradient method, we modify shifts $r(\tau, l)$ after CG iterations are complete to satisfy this constraint. A better approach is to find a constrained least-squares solution that satisfies the monotonicity constraints. Constrained least-squares methods exist, but are more complex than the method used here.

REFERENCES CITED

- Beyer, L.A., & Clutson, F.G. 1978. *Density and porosity of oil reservoirs and overlying formations from borehole gravity measurements, Gebo Oil Field, Hot Springs County, Wyoming*. Tech. rept. United States Geological Survey.
- Compton, S, & Hale, D. 2013. *Estimating Vp/Vs ratios using smooth dynamic image warping*. Tech. rept. CWP - 765. Colorado School of Mines.
- Doveton, John H. 1994. *Geologic log analysis using computer methods*. American Association Of Petroleum Geologists.
- Fang, J. H., & Chen, C. 1992. Computer-aided well log correlation. *The American Associate of Petroleum Geologists Bulletin*, **76**, 307–317.
- Hale, Dave. 2013. Dynamic warping of seismic images. *Geophysics*, **78**(2), S105–S115.
- Harlan, William S. 1995. *Regularization by model reparameterization*. <http://billharlan.com/pub/papers/regularization.pdf>.
- Kovalevskiy, E. V., Gogonenkov, G. N., & Perepechkin, M. V. 2007. Automatic well-to-well correlation based on consecutive uncertainty elimination. *In: 69th EAGE Conference and Exhibition, London, Extended Abstracts*.
- Lallier, F., Caumon, G., Borgomano, J., & Viseur, S. 2014. Uncertainty assessment in stratigraphic well correlation of a carbonate ramp: method and application to the Beausset basin, SE France. *In: Second EAGE Integrated Reservoir Modelling Conference*.
- Le Nir, I, Van Gysel, N, & Rossi, D. 1998. Cross-section construction from automated well log correlation: a dynamic programming approach using multiple well logs. *In: SPWLA 39th Annual Logging Symposium*.
- Lineman, D.J., Mendelson, J.D., & Toksöz, M.N. 1987. Well-to-well log correlation using knowledge-based systems and dynamic depth warping. *In: SPWLA 28th Annual Logging Symposium*.
- Loeff, Kurt M. 2001. The application of geophysical borehole logging as it pertains to the geologic characterization of salt storage, reservoir storage and brine disposal. *In: SMRI Shortcourse on Geophysical Borehole Methods*.

- Rudman, A. J., & Lankston, R. W. 1973. Stratigraphic correlation of well-logs by computer techniques. *American Association of Petroleum Geologists Bulletin*, **57**, 577–588.
- Sakoe, Hiroaki, & Chiba, Seibi. 1978. Dynamic programming algorithm optimization for spoken word recognition. *IEEE Transactions on Acoustic, Speech, and Signal Processing*, **ASSP-26**(1), 43–49.
- Smith, T, & Waterman, M. 1980. New stratigraphic correlation techniques. *Journal of Geology*, **88**, 451–457.
- Wu, X, & Nyland, E. 1987. Automated stratigraphic interpretation of well-log data. *Geophysics*, **52**, 1665–1676.